X-RAY DIFFRACTION STUDIES ON THE CROSS-SECTIONAL STRUCTURE OF SALMONELLA FLAGELLA

TAKASHI YAMAGUCHI

Department of Biophysical Engineering,
Faculty of Engineering Science,
Osaka University

Table of Contents

Abstract

X-ray diffraction studies have been made on the cross-sectional structure of the normal Salmonella flagella, putting special emphasis on the number of constituent strands. Two approaches have been made: one based upon moderate-angle equatorial diffractions ($12° > 2\theta \geqslant 3°$) and the other upon small-angle equatorial scatterings ($2\theta < 3°$).

In the investigation of the moderate-angle diffraction pattern, validity is examined of the model that the flagellum consists of annularly arranged strands, of which each has a cylindrically symmetric structure. Main features of the pattern can be interpreted by this model. Obtained results suggest that the flagellum consists of 11 strands, supporting the conclusion of O'Brien and Bennett (1972) based upon optical diffraction studies of electron micrographs.

Cylindrically averaged electron density of the cross section of flagellum is obtained by means of the Fourier-Bessel transformation method on the basis of the small-angle scattering measurements. The density distribution shows that the average radius of flagellum is about 65 Å and there exist a low density region with radius of about 15 Å at the centre of flagellum. The value of average radius also is favorable for the model that the flagellum consists of 11 strands.

Chapter 1. Introduction

Recently structure and function of bacterial flagella have been intensively studied as reviewed in references.[1-6] The flagellum is a motile organelle and compries at least three parts which can be distinguished in the electron microscope: a basal portion connected with the cytoplasmic membrane, a proximal hook and the main herical filament, according to Abram, Koffler and Vatter.[7] Below we shall call this main helical portion as flagellum. The present study has been made on Salmonella flagella of the normal type. They are long filaments (up to 10 μ) of uniform diameter of about 200 A and helix-shaped with the wave length of 2.5 μ. They consist of protein molecules called flagellin, which has molecular weight of about 40,000. According to the investigations by electron microscope (Kerridge, Horne and Glauert,[8] and Lowy and Hanson[9] and X-ray diffraction (Champness and Lowy,[10] Champness[11] and Wakabayashi and Mitsui[12]), the flagella are composed of longitudinal rows consisting of approximately globular flagellin molecules. The rows are called strands. There have been various proposals on the number of strands.[9,13-17] Lowy and Hanson[9] estimated it as 7-10 based upon their electron micrographs and proposed a model consisting of 8 strands which is shown in Fig.1(a). Recently, however, O'Brien and Bennett[15] have made optical diffraction studies on electron micrographs and concluded that it is 11 for the straight Salmonella

flagella. On the basis of the same method, Champness[11] concluded that it is 8-10 in favor for the conclusion of Lowy and Hanson.[9] Finch[16] and Finch and Klug[17] studied the superposition patterns of electron micrographs of a flagellum tilted by 15° intervals about its axis. They concluded that the number of strands is 11 for Salmonella flagella[16,17] and also for other species[17] (Pseudomonas flurorescens, Bacillus subtilis). On the basis of small-angle X-ray, Bode et al.[19] concluded that the number of the strands is 8-10 from the mass per unit length of Proteus flagella. According to them, the flagellin molecules are elongated and the Lowy-Hanson's model should be modified as shown in Fig.1(b). Hitherto, however, so much emphasis has not been put on the number of strands in the X-ray diffraction studies as the optical diffraction studies of electron micrographs, and more detailed X-ray studies seem to be needed.

In the present study, cross-sectional structure of normal Salmonella flagella has been studies, putting special emphasis on the number of the constituent strands. Two approaches have been made: one based upon the moderate-angle equatorial diffractions ($12^\circ \geqslant 2\theta > 3^\circ$) and the other upon small-angle equatorial scatterings ($2\theta < 3^\circ$). In the analysis of the moderate-angle diffraction pattern, validity is examined of the model that the flagellum consists of annularly arranged strands, of which each has a cylindrically symmetric structure.[20-23] On the basis of

the small-angle scattering measurements, cylindrically averaged electron density of the cross section of the flagellum is obtained by means of the Fourier-Bessel transformation method, which was originally proposed by Franklin and Holmes[24] and Fedrov.[25]

Chapter 2. Materials and Methods

§ 2-1. Preparation of flagella

Flagella were obtained from Salmonella strain SJ25, of which flagella have normal helical form.[26] Cultivation of the organisms and the isolation and purification of flagella were carried out by the method described by Kerride et al.[8] and Asakura et al.[27,28] Salmonella were precultured for 12 hr at 35°C in 150 ml solution containing 1.5 g peptone and 1.5 g yeast extract and then were cultured in large quantities, for 8 hr at 35°C with airation in a 5 l medium solution containing 50 g peptone, 25 g yeast extract, 25 g beef extract, 200 ml phosphate buffer (1 M, pH 7.8) and 15 g glucose. After collecting bacterial cells and washing with distilled water, flagella were isolated by shaking. Collected flagella were washed with a solution containing 0.15 M NaCl and 10 mM phosphate buffer (pH 7.0). Obtained flagella were purified by depolymerization and polymerization processes.[27,28] Fig.2 and 3 show the flow charts for preparation and purification of flagella, respectively. Plate I shows an electron micrograph of Salmonella flagella used in the present study.

§ 2-2. Preparation of X-ray specimens

Opalescent flagellar pellets of a consistency suitable for making oriented fibre specimens were obtained from an

aqueous flagellar suspension, containing approximately 3 mg protein/ml., by ultracentrifugation at about 100,000 g for 1 hr. The oriented fibre specimens were obtained by allowing a flagellar pellet to dry slowly between two glass rods.[11,12,29,30] The width of the fibres prepared in this way was about 0.5 mm. Humidity was controlled by saturated KNO_3 solution in the case of fibre specimens and relative humidity was about 93 %. Solution specimens were obtained by dilution of concentrated flagellar solution. The concentration of a flagellar solution, C, was determined by the biuret reaction with optical density measurements.

$$C = \frac{1}{0.059} \times \frac{OD}{\ell} \qquad \text{(mg protein/ml)}$$

Here, ℓ is the optical length (cm) and OD is the optical density at the wave length of 530 mμ. X-ray studies on solution specimens were carried out in the concentration range from 5 mg protein/ml to 50 mg protein/ml.

§ 2-3. X-ray methods

Moderate-angle X-ray diffraction patterns ($12° \geqslant 2\theta > 3°$) were obtained by the toroidal mirror collimating camera[31] with Fuji Medical films. Nickel-filtered CuKα radiation from Rigaku Denki rotating anode microfocus generator was used. Diffraction spacings were calibrated with $(NH_4)_2SO_4$ powder patterns. The darkness of the photographs was read with Narumi microphotodensitometer

and the scattering intensities were obtained with correction of the linearity of the darkness. The correction was performed by the calibration table relating the darkness to the exposure time. For smaller angle than 3° X-ray scattering intensities were measured using a Rigaku Denki small-angle X-ray collimater with line slits and a proportional counter with a single channel differential pulse height analyser, monitoring the fluctuation of a X-ray source by a Geiger-Müller counter. Solvent scattering was measured and substracted from solution scattering. Collimation effects caused by the line shaped geometry could be eliminated by use of the Fortran program made by P. W. Schmidt (1967),[32] which was kindly supplied by Dr. K. Miyake (Department of Polymer Science, Hokkaido University). Calculations were carried out on the NEAC 700 Computer of the Computer Centre of Osaka University.

Chapter 3. Experimental Results

X-ray diffraction intensities were obtained for three kinds. One of them was small-angle X-ray scattering of the flagellar solution. A second was moderate-angle X-ray diffraction of the solution and a third was moderate-angle equatorial X-ray diffraction of the oriented fibre specimen. Small-angle X-ray scattering experiments were planned in order to determine the cylindrically averaged electron density of the flagellum and also in order to investigate the interference effects between flagella with varying concentration of flagellar solutions. The equatorial X-ray diffraction from oriented fibre specimens was the most important for the present analysis to determine the arrangement of the strands in a flagellum. Moderate-angle X-ray diffraction experiments of solutions were the supplemental ones in order to investigate the interference effect between flagella in the moderate-angle region, comparing with the X-ray patterns of fibre specimens.

§ 3-1. Small-angle X-ray scatterings

In Fig.4, the small-angle X-ray scattering intensity of flagellar solutions is shown in a logarithmic scale. The abscissa is the absolute value of reciprocal vector R, which is related to scattering angle 2θ, and wave length λ of CuKα radiation, by $R=2\sin\theta/\lambda$. The X-ray scattering

intensities from aqueous solutions are spherically averaged, so it is necessary to transform them to cylindrically averaged intensities.[40] This correction is performed by multiplying scattering angle. Therefore the ordinate of Fig.4 is the product of observed intensity and scattering angle.

§ 3-2. Moderate-angle X-ray diffractions

For larger scattering angle than 3° ($R \geqslant 1/29.4\ A^{-1}$), Plate (2a) and Plate (2b) show X-ray diffraction patterns from fibre specimens and aqueous solutions, respectively. The observed spacings of equatorial diffraction peaks for each case are listed in Table I. In the X-ray patterns of aqueous solutions, both equatorial and other layer reflections are overlapped. The distinction between equatorial patterns and other layer ones were achieved by comparison with the diffraction patterns from oriented fibre specimens. In Table I, other layer reflections are in brackets. The angular spread of each reflections of fibre patterns comes from the distribution of the orientation of the flagella in the specimens. This angular spread is smearing each reflection. So, the intensity correction is necessary. The correction was achieved by multiplying scattering angles, since the angular spread is increased with linear relation to the scattering angle. After this correction, the both diffraction intensities are

shown in Fig.5, where full line is for fibre specimens and dotted chain line is for aqueous solutions.

Chapter 4. Fundamentals of Analysis

§ 4-1. Theoretical bases on equatorial X-ray diffraction intensities

The equatorial X-ray diffraction intensity from oriented fibre specimens is given by the following expression,[33]

$$I(R) = \sum_n \left| \int_0^\infty \rho_n(r) J_n(2\pi Rr)\, 2\pi r dr \right|^2. \qquad (1)$$

Here, $\rho_n(r)$ is the Fourier coefficient of the electron density projected onto (r,ϕ) plane along z-axis in cylindrical coordinates, where the z-axis is taken along the fibre axis. $J_n(2\pi Rr)$ is the n-th order Bessel function. The radial component, R, of the reciprocal vector is related to the scattering angle, 2θ, and the wave length of X-ray, λ, by the equation, $R=2\sin\theta/\lambda$. Eq.(1) can not be solved directly, so it must be necessary to approximate them in order to reduce the integrals. One approximation proposed by Franklin and Holmes[24] and Fedrov[25] is that the fibre under consideration is approximated to the cylindrical symmetric one. Then, the diffraction intensity is simplified.

$$I(R) = \left\{ \int_0^\infty \rho(r) J_o(2\pi Rr)\, 2\pi r dr \right\}^2 \qquad (2)$$

and the electron density is obtained directly by the inverse Fourier-Bessel transformation.

$$\rho(r) = \int_0^\infty \pm\sqrt{I(R)}\; J_o(2\pi Rr)\, 2\pi R dR. \qquad (3)$$

The average radius is defined as

$$\bar{r} \equiv \int r\rho(r)2\pi r dr / \left\{\int \rho(r) 2\pi r dr\right\}. \quad (4)$$

The radius of gyration of the cross section R_q is defined by

$$R_q^2 \equiv \int r^2 \rho(r) \cdot 2\pi r dr / \left\{\int \rho(r) 2\pi r dr\right\}. \quad (5)$$

When R is small, the term concerning the O-th order Bessel function in Eq.(1) is dominant compared to other orders because the only O-th order Bessel function has finite value at R=0 and others go to zero. So the small-angle X-ray diffraction intensities can be analyzed by Eq.(2) and Eq.(3) with good approximation.

On the other hand, at the region of larger scattering angles, it is necessary to consider the angular dependence of the electron density, that is, other terms of Eq.(1) can not be neglected. Another approximation can be developed as was done by Oster and Riley.[20-23] It is that the inner structure of fibrous systems is approximated to the assembly of cylindrical strands. The representation of the diffraction intensity is also simplified.

$$I(R) = f^2(R) \sum_i^N \sum_j^N J_o(2\pi R r_{ij}). \quad (6)$$

$f^2(R)$ is the molecular scattering intensity of strands and r_{ij} is the distance from the i-th strand to the j-th one. The number of strands in a fibrous system is N. An Interference function, i(R), can be introduced,[34]

$$I(R) = Nf^2(R) i(R) \quad (7)$$

$$i(R) = 1 + \frac{1}{N} \sum_{i \neq j} J_o(2\pi R r_{ij}) \quad (8)$$

A radial distribution function,[35] $p(r)$, is obtained with the Fourier-Bessel transformation from the interference function,

$$p(r) = \int_0^\infty i(R) J_o(2\pi Rr) 2\pi R dR \tag{9}$$

Putting Eq.(8) to Eq.(9), then

$$p(r) = \delta(r) + \frac{1}{N} \sum_{i \neq j} \delta(r-r_{ij}). \tag{10}$$

Here, $\delta(r) = \int_0^\infty J_o(2\pi Rr) 2\pi R dR$,
and $\delta(r-r_{ij}) = \int_0^\infty J_o(2\pi Rr_{ij}) J_o(2\pi Rr) 2\pi R dR$.
Both $\delta(r)$ and $\delta(r-r_{ij})$ are Dirac's δ-functions in two dimensional space (r,ϕ). So the radial distribution function, $p(r)$, has sharp peaks at the positions corresponding to the lengths of the distances between strands. The first term in Eq.(10) is usually omitted.[34] Because it is a self-evident peak and any informations from it can not be available for the analysis of the arrangement of the strands composing the systems under consideration. Then, the Fourier-Bessel transformation is achieved against $i(R)-1$ and Eq.(8) is rewritten followingly,

$$p'(r) = \int_0^\infty (i(R) - 1) J_o(2\pi Rr) 2\pi R dR. \tag{11}$$

§ 4-2. Empirical method to determine molecular scattering factors and interference functions

In order to determine the radial distribution function, it is necessary to know the molecular scattering

intensity of the strands. When strands are composed from protein molecules, as bacterial flagella, the calculations of the molecular scattering intensities are impossible at present. Because protein molecules generally have complex inner structures. Therefore it is demanded to develope the appropriate method to choose the molecular scattering intensities. We propose the empirical method to estimate them, based on the properties of interference functions for 2-dimensional arrays and also general features of scattering intensities of protein.

The most important property of the interference function for the present case is that interference functions oscillate around unity as a whole and the oscillations are damping toward the limitting value, that is, unity, with R going to infinite. This property is obvious from Eq.(8). The second term of Eq.(8) is the sum of the O-th order Bessel functions, which are the functions of oscillation with damping to zero. The damping oscillation of the interference function is sufficient at large reciprocal region.

On the other hand, concerning molecular scattering intensities of proteins, it is well known that the molecular scattering intensities of protein molecules usually have a smooth peak positioned at about 1/10 $\mathring{A}^{-1}$. [36-38] Arndt and Riley[36] observed spherically averaged intensity curves from many kinds of protein molecules in the dried amorphous state. They showed that the intensity

curves fall into only three essentially different types, called α, β and γ, and these have scattering maxima near the reciprocal length of 1/10 $\mathring{A}^{-1}$. They attributed these peaks to the packings of polypeptide chains in protein molecules. The position of these peaks and relative intensities rather varies, characteristic to individual proteins. But this is the most prominent property of the molecular scattering intensity of the protein molecules in the moderate-angle region.

According to Eq.(7), diffraction intensities are represented by the product of interference functions and molecular scattering intensities. So, it is expected that the diffraction intensities have the profile of damping oscillation around the curves which have a smooth peak near 1/10 $\mathring{A}^{-1}$. This profile can be seen actually in the diffraction intensity obtained for Salmonella flagella (see below). Inversely, it could be proposed that the molecular scattering intensity is determined by the procedure of smoothing of the oscillation of the observed diffraction intensity. Then the interference function can be obtained with dividing the observed diffraction intensity by this estimated molecular scattering intensity. Consequently, obtained interference function has the profile of the damping oscillation around unity. The procedure of smoothing is rather arbitrary. But the uncertainty is not severe since the positions of peaks of finally obtained radial distribution functions are not affected (see

Appendix I). From the standing point of the methodological generality, we averaged two smooth curves, one of which is linked the portions of the peaks of diffraction intensity curve and another is linked the portions of the bottoms. The errors introduced by this empirical method and utilities were examined in Appendix I and II.

§ 4-3. Effects of positional fluctuations

There may be some distortions or positional fluctuations in the arrangement of the strands in a system. The distortion of the arrangement is assumed to Gaussian distribution function.

$$g(r) = \frac{B^2}{\pi} \exp(-B^2 r^2) \tag{12}$$

Here, B is related to the standard deviation, ϵ, of the distortion of the arrangement, as $B=1/\sqrt{2}\epsilon$. Then, the interference function is modulated as follows,

$$i(R) = 1 + \left\{\exp\left(-\frac{\pi^2}{B^2}R^2\right)\right\}\frac{1}{N}\sum_{i\neq j} J_o(2\pi R r_{ij}) \tag{13}$$

So, the mean decay toward unity of the interference function is attributed to two factors, one of which is the damping oscillation of Bessel functions and another is the Gaussian decay by the distortion. The oscillating terms by Bessel functions decay with $R^{-\frac{1}{2}}$, approximately.[39] The additive exponential term quenches the amplitude of the interference function than $R^{-\frac{1}{2}}$ rule. By plotting absolute

value of $R^{\frac{1}{2}}(i(R)-1)$ versus R^2 on logarithmic scale, it is possible to estimate the standard deviation of the distortion from the slope of these plottings. But if the strands in a fibrous system deviate from cylindrical symmetry, there apears other damping factor due to asymmetry (see Appendix II). Therefore, the standard deviations obtained by these plottings are mean values of the superposition of the distortion and asymmetry, which we shall call equivalent standard deviation.

Chapter 5. Analysis of Small-Angle X-Ray Data

The radius of gyration of the cross section of the flagella R_q, given by Eq.(5), is related to the initial slope tan α of the Guinier plot,[41] which is illustrated in Fig.6.

$$R_q = 0.342\sqrt{\tan \alpha}$$

In Fig.6 small concentration dependence of the scattering curves had been eleiminated by extrapolation to zero concentration. The ordinate is also the product of scattering intensities and scattering angle as mentioned in Chapter 4. From Fig.6 we have R_q=68 Å. Using the radius of gyration of cross section hollow cylinder models were examined. The inner and outer radius, r_1 and r_2, of the hollow cylinders are related to the radius of gyration, R_q.[19]

$$R_q^2 = (r_1 + r_2)^2/2.$$

If the ratio of the inner to outer radius, r_1/r_2, is determined, r_1 and r_2 are calculated. r_1/r_2 was determined from the ratio of the scattering intensity at the origin to the intensity at the 1st subsidary peak of R=0.009 $Å^{-1}$. The peak value at the origin could be obtained by the extrapolation of the scattering curve of Fig.6 to zero. The ratio of it to the peak value of the 1st subsidary one was about 40. This value was compared with the values of theoretical curves calculated for full and hollow cylinders

varying the ratio of inner to outer radius of hollow cylinders.[33] As a result, it corresponded to the hollow cylinder with the ratio of inner to outer radius, r_1/r_2, of 0.16. From both R_q and r_1/r_2, r_1 and r_2 were obtained as,

$$r_1 = 15 \text{ Å},$$

and

$$r_2 = 95 \text{ Å}.$$

The average radius of this hollow cylinder could be calculated by Eq.(4) and was 65 Å.

From the total intensity curve of Fig.4, the cylindrically averaged electron density was obtained using the inverse Fourier-Bessel transformation, Eq.(3). The results are shown in Fig.7, here the phases of each scattering peaks were assumed as (+,-,+) in (a) and (+,-,-) in (b) for the principal peak at the origin and two subsidary peaks. In this integral, the third peak of which spacing is 1/47 $Å^{-1}$ was omitted. Because it was made clear that this reflection is originated from the first layer line, judging from X-ray patterns of oriented fibre specimens. Other phase combinations may be also possible but the present combinations were consistent with moderate-angle X-ray diffraction studies. Obtained electron density shows that Salmonella flagella have the outer radius of about 100 Å with low electron density core at the centre of radius of about 15 Å. And there exists the maximum of the electron density near the radius of 50 Å. The average

radius was calculated and was 65±5 Å. These agree with the hollow cylinder model, which is mentioned above.

Chapter 6. Analysis of Moderate-Angle Equatorial X-Ray Data

§ 6-1. Effects of interference between flagella

Before the calculations, it must be necessary to identify the origins of each reflections, that is, which the reflections originate from the intra-flagellum or inter-flagella interference, since the equatorial reflections which are originate from the intra-flagellum interference are only needed to elucidate the lateral structure in the flagellum.

In the experiments of X-ray diffraction of flagellar solutions, the interference effect between flagella can be eliminated by dilution of solutions. So, the change of the profile of the diffraction intensities was examined by varying the concentration of the solution. Consequently, in the concentration range from 5 mg/ml to 50 mg/ml, there was no change in profiles for the scattering angle larger than 0.5°. From this fact, the interference effect between flagella can be neglected against these regions for solution patterns.

The interference effect between flagella of the equatorial patterns from the fibre specimens were investigated from the comparison with diffraction patterns from aqueous solutions, and from the experiments of changes of humidity. Comparing diffraction patterns from fibre

specimens and solutions, most of spacings of the equatorial reflections of fibre patterns corresponded to those of solutions (see Table I). The relative intensities of each reflection for both cases are rather different (see Fig.5) but the differences are unavoidable because of the facts that the diffraction patterns from solutions contain both equatorial and other layer reflections. On the other hand, when the fibre specimens were allowed to dry in vacuum from relative humidity of 94 %, the profile of small-angle equatorial patterns were very different from those of solution but moderate-angle equatorial reflections ($2\theta \geqq 3°$) remained. Only the spacings decreased about 1-3 % than the case of the relative humidity of 94 %, as was observed by Champness[11] and Burge and Draper[42]. Considering together, the interference effects seem to be also negligible in the case of the fibre specimens for the region of the scattering angle larger than 3°.

§ 6-2. Calculation of the radial distribution function

Moderate-angle equatorial X-ray diffraction patterns from oriented fibre specimens were analyzed quantitatively using a radial distribution function as mentioned above. In order to apply this method, three steps are necessary. The first step is the determination of the molecular scattering intensity of the strands composing the flagellum and the second step is the calculation of the interference

function. The last step is the calculation of the radial distribution function from the interference function by the Fourier-Bessel transformation.

The molecular scattering intensity, $f^2(R)$, was determined by the above mentioned empirical method. In Fig.8, the obtained molecular scattering intensity of the strands are shown. Here, the full line is the observed intensity and dotted chain line is the molecular scattering intensity of the strand, obtained by averaging two smooth curves shown as dotted lines.

The interference function, i(R), in Eq.(7) was calculated by dividing observed intensity curve by the estimated molecular scattering intensity of the strand. The result is shown in Fig.9. The obtained interference function has the profile of the oscillation with damping toward unity as mentioned. The average decay toward unity is fast. The fast decay is attributed to two factors, one of which is concerned to the distortion in the position of the strands in a flagellum, as mentioned above. Another is due to the asymmetry of the strands (see Appendix II). The equivalent standard deviation under Gaussian approximation can be estimated from the mean decay of $\log(|R^{1/2}(i(R)-1)|)$, versus R^2, which is shown in Fig.10. As a result, it was $3 \sim 4$ Å.

At the third step, the radial distribution function, p'(r) given by Eq.(11), was calculated from the interference function. Fig.11 shows the radial

distribution function calculated from the interference function shown in Fig.9. In this calculation, ripples due to terminated integral of Eq.(11) were smeared by the artificial temperature factor.[43] The termination errors is originated from slow conversion of Bessel function in Eq.(11). Hence, the ripple can be eliminated by multiplying the attenuation factor to $J_o(2\pi Rr)$. Usually the attenuation factor is taken a form of $\exp(-\text{const.}\times R^2)$, as temperature factors in X-ray crystallography, so-called artificial temperature factor. There exist several peaks at radial vector lengths of 11Å, 24Å, 35.5Å, 50Å, 70Å, 85Å, 98Å and 125Å. Among these peaks, four peaks are especially clear. They are at 35.5Å, 70Å, 98Å and 125Å, as seen in Fig.11. Hereafter, these four peaks are called clear peaks and other peaks, positioned at 11Å, 24Å, 50Å and 85Å are called as sub-peaks.

§ 6-3. Number of strands and their arrangement

The positions of the peaks of the radial distribution function correspond to distances between the strands in a flagellum. The relative arrangement of the strands is examined, based on the radial distribution function, particularly paying attentions to the radial distances of clear peaks at 35.5Å, 70Å, 98Å and 125Å. Other peaks called sub-peaks are assumed to be caused by asymmetries of strands as described in Appendix II. In the clear peaks, the distance of 35.5Å seems to correspond to the nearest

neighbour distance between strands in a flagellum. The geometrical construction of the arrangement of strands in a flagellum was done using this nearest neighbour distance as following procedure: At first, a strand was fixed at the origin of a space and the second one was put on a point separated from the origin with the distance of 35.5Å. Then, the position of the third one was determined from the intersecting point of the two circles, one of which was centred at the origin and the radius of 70Å and another of which was centred at the position of the second strand with radius of 35.5Å and so on. From these geometrical construction, the possibility of the arrangement of the strands was restricted to the annular array in a flagellum. The number of the strands of the annular array could be equal or greater than 11.

Further examinations were achieved with comparing the obtained radial distribution function and calculated ones for several annular arrays. In Fig.12, only positions of the peaks for each one are shown. The calculations were with fixing the nearest neighbour distance at 35.5Å. The abscissa is the number of the strands of annular models. Circles indicate the positions of the peaks of the calculated radial distribution function. Horizontal full lines and dashed lines indicate the positions of clear peaks of Fig.11 and breadth for each peak, respectively. The agreement between them is well sufficient when the number of the strands is greater than or equal to 11.

For these models, we calculated the moderate-angle equatorial diffraction intensity using the estimated molecular scattering intensity of strands of Fig.8. In the calculations, the damping factor was considered according to Eq.(13), estimated as above. Fig.13 shows calculated intensities for 8, 11 and 13 strands models of the nearest neighbour distance of 35.5 Å with the equivalent standard deviation of 4 Å. By virtue of the equivalent standard deviation, there are some discrepancies between observed and calculated intensities for each case in the region that $R \geqslant 0.1$ Å^{-1}. This may be due to the deviation from the cylindrical strand approximation (see Appendix II). However, the peak positions of the observed diffraction intensity coincide with those of the 11 strands model as a whole. Further, the discrepancy factor for the interference function was calculated according to the following.

$$\Delta = \frac{\int |i_N(R) - i(R)| \, dR}{\int i(R) \, dR}$$

Here, $i_N(R)$ is the interference function of the N strands annular array, and $i(R)$ is same as shown in Fig.9. The results of the calculations are illustrated in Fig.14, which shows that the best fit is obtained surely for the 11 strand model. At last, the calculated intensity for the 11 strands model with the equivalent standard deviation of 3 Å are indicated in Fig.15.

Chapter 7. Discussion

As discussed above, a normal Salmonella flagellum seems to consist of 11 longitudinal strands separated by distance of 35.5 Å. This implies that the centres of strands are situated on a cylinder of which radius r_o is given by $2r_o\sin(\pi/11)=35.5$ Å. The value of r_o obtained is 63 Å. The distance between the centres of neighbouring flagellin molecules on one strand is 51.9 Å according to Wakabayashi,[44] who estimated it from meridional diffraction patterns of normal Salmonella flagella. Fig.16 shows the side view of flagella as a summary of the above-mentioned results. The circles stand for flagellin molecules. Here, the radius of the circles has no exact physical meaning through they were drawn as a/2, whereas their centres has definite meaning. The structure is characterized by the parameters a, b and γ as shown in Fig.16, which can be determined by geometrical consideration and are 46 Å, 51.9 Å and 128°, respectively.

Fig.17 shows the top view of a flagellum. In Chapter 5 we determined the electron density $\rho(r)$ of flagellum and the average, inner and outer radii $\bar{r}$, r_1 and r_2 on the basis of small-angle scattering data. The radii r_1 and r_2 were defined referring to the uniform density model. These radii also are shown in Fig.17. It should be noticed that the obtained $\bar{r}$ is nearly equal to r_o. As mentioned above, the radius of the circles representing each flagellin molecules has no exact meaning. Thus the curve $\rho(r)$ seems

to give a picture which is closer to the reality concerning the cylindrically averaged density distribution. This $\rho(r)$, along with the inner and outer radii r_1 and r_2, suggests that the thickness of a flagellum is larger than the nearest neighbour distance of flagellin molecules and that an actual flagellin molecule has a shape elongated radially as discussed by Bode et al.[19] Also Fig.16 suggests that the monomers has a shape elongated along the flagellar axis. Effects of the deviation of monomer shape from the spherical symmetry in the projected plane on the moderate-angle diffraction pattern are examined for symplified models in Appendix II. The conclusion is that the deviation does not affect the positions of the centres of gravity of monomers determined referring to the main peaks on the radial distribution functions, if the deviation is moderate. This seems to be our case because numerically we have obtained the relation $\bar{r} \approx r_o$.

Bode et al.[19] studied the small-angle scatterings from Proteus flagella and obtained the following values of structural parameters: R_q=56 Å, r_1=15 Å, r_2=73 Å. The average radius $\bar{r}$ calculated by us for their model is 50 Å. These may be compared with our results on Salmonella flagella: R_q=68 Å, r_1=15 Å, r_2=95 Å, $\bar{r}$=65 Å. Therefore, the Salmonella flagella are thicker than the Proteus flagella.

In conclusion, our X-ray studies shows that the number of longitudinal strands in a flagellum of Salmonella strain

SJ25 is most possibly 11 in agreement with the conclusions of Finch[16] and Finch and Klug[17] and O'Brien and Bennett.[15] Recently Furuya[45] in this laboratory made electron microscopic studies of Salmonella flagella by means of a computer-processed Fourier transform method and obtained results favorable to our conclusion.

Chapter 8. Summary

(1) Small-angle X-ray scatterings of a solution of flagella of Salmonella strain SJ25 were measured for scattering angle, $0.2° \leqslant 2\theta \leqslant 3°$. Intensity measurements were made by the counter method in the range of the concentration of solution, 5 ~ 50 mg protein/ml.

(2) Moderate-angle equatorial diffraction patterns from oriented fibre specimens were recorded by the film method using the toroid optics. Diffraction intensities on the equator were measured with the densitometer for scattering angle, $3° \leqslant 2\theta < 12°$.

(3) In the same moderate-angle, $3° \leqslant 2\theta < 12°$, diffraction intensities were obtained for aqueous solution. Comparing fibre patterns with solution patterns, it was concluded that the effects of interference between flagella in the fibre specimen can be neglected.

(4) From small-angle X-ray data, the electron density distribution of the cross-section were obtained, as shown in Fig.7. The average radius was calculated from the electron density as 65 Å. The structural parameters of a hollow cylinder model for the cross-section were obtained: the radius of gyration as 68 Å and the inner and outer radius as 15 Å and 95 Å.

(5) In studies on the moderate-angle equatorial diffractions, an approximate method was proposed, in which the intensity is expressed by the product of the molecular scattering intensity of each strand and the

interference function of the assembly of the strands in a flagellum. The validity of this approximation were examined by model calculations in Appendices.

(6) Applying this approximate method, the radial distribution function of strands in a flagellum was determined. It proved that the centre-to-centre distance between the nearest strands in a flagellum is 35.5 Å and the number of the strands is equal to or greater than 11.

(7) For several models having different number of strands, the equatorial diffraction intensities were calculated using the empirically determined molecular scattering intensity of the strand, and examined which model gives the best fit. The discrepancy factor for the interference function of the models were also calculated. Obtained results suggested that the number of strands is 11, supporting the conclusion of Finch,[16] Finch and Klug[17] and O'Brien and Bennett[15] based upon the electron microscopy.

(8) The radius of 11 strands model determined as 63 Å is in good agreement with the average radius 65 Å obtained from small-angle X-ray studies, indicating that both approaches based upon the small- and moderate-angle X-ray scatterings are reasonablly reliable.

(9) Results of both small- and moderate-angle studies suggest that the shape of the flagellin molecule considerably deviates from a spherical symmetry in

accordance with the conclusion of Bode et al.[19]

Acknowledgment

The author is greatly indebted to Prof. T. Mitsui for his helpful discussions and encouragements throughout this study. He also wish to express his thanks to Dr. K. Wakabayashi for valuable discussions and assistances in this experiment and to Mr. K. Furuya for taking the electron micrographs. His thanks are due to Dr. T. Ueki, Dr. T. Hamanaka and other members in this laboratory for valuable discussions.

APPENDIX I. Ambiguities of the Empirical Method

When the fibrous system consists of same kinds of structural units (strands), assuming the cylindrical symmetry of the strands, equatorial X-ray diffraction intensity, I(R), is represented as follows.[33]

$$I(R) = Nf^2(R)i(R), \tag{A1}$$

$$i(R) = 1 + \frac{1}{N}\sum_{i\neq j} J_o(2\pi R r_{ij}). \tag{A2}$$

Here, N is the number of the strands in a fibrous system, $f^2(R)$ is a molecular scattering intensity of a strand and i(R) is the interference function for the arrangement of the strands. r_{ij} is the distance between the i-th strand to the j-th one and $J_o(2\pi R r_{ij})$ is the O-th order Bessel function. A radial distribution function, p(r), is calculated from i(R) by the Fourier-Bessel transformation.

$$p(r) = \int i(R) J_o(2\pi R r) 2\pi R dR, \tag{A3}$$

or

$$p'(r) = \int (i(R) - 1) J_o(2\pi R r) 2\pi R dR. \tag{A4}$$

In p'(r), the peak at the origin is omitted, as usual.[34] In order to calculate p(r) or p'(r), it is necessary to extract i(R) from I(R) in Eq.(A1).

We proposed the method to determine the molecular scattering intensity and the interference function from the observed diffraction intensity, that is to say, the molecular scattering intensity was obtained by smoothing

the oscillation of the intensity curves. Consequently, the interference function obtained by this method must be oscillate around unity. This empirical method is based on the general properties of the interference functions and molecular scattering intensity of protein: (1) The interference functions oscillate around unity and damp toward it as a whole, and (2) the molecular scattering intensity of protein molecules has a smooth peak near the reciprocal vector length of 1/10 A^{-1}. Fig.A1 shows the interference functions for three typical arrays for the case of 6 strands. The abscissa is reduced reciprocal vector length, $u=2\pi Ra$, here a is the nearest neighbour distance between strands.

However, the property of the damping oscillation around unity breaks down at small reciprocal region, so that the systematic errors may be introduced to the interference function at these regions. Now we discuss the effects of the erroneous interference function originated to the deviation from the damping oscillation property.

The interference function obtained by the empirical method, $i_{emp}(R)$, can be represented by the product of true interference function, $i(R)$, and the error function, $w(R)$,

$$i_{emp}(R) = i(R) \cdot w(R). \qquad (A5)$$

The effect of the systematic errors on the radial distribution function were investigated by comparison with radial distribution functions obtained from $i(R)$ and

$i_{emp}(R)$. The error-function was put as follows, since the errors due to the deviation from damping oscillation around unity become large when R goes to zero.

$$w(R) = A(R - R_o)^2 + 1, \quad R < R_o,$$
$$= 1 \quad , \quad R > R_o. \tag{A6}$$

About many values for parameters of A and R_o, the effects were examined systematically. For example, these are shown in Fig.A2 and Fig.A3. In Fig.A2, the interference function which containes the systematic errors are shown; (———), true interference function for the annular array of 6 strands; (— + —), u_o=12, $A=1/u_o^2=1/144$; (— − —), u_o=12, A=-1/144. The abscissa is reduced reciprocal vector length. Fig.A3 shows the radial distribution functions obtained from these interference function, respectively. The abscissa is reduced radial distance, x=r/a, here r is the radial distance and a is the nearest neighbour distance. The annular array with 6 strands has three kinds of inter-strands distances, that is, a, $\sqrt{3}$a, 2a. These values correspond to x=1, $\sqrt{3}$, 2, respectively. These peaks are shown in Fig.A3. It is shown that the systematic errors take no effects on the peak positions of the radial distribution functions. They affects only on the base line with slowly changed manner. These effects are commonly observed until for rather large values of u_o up to 60, and also for other arrays and the number of strands. From this fact it could be concluded that it is not severe, so long

as the positions of the peaks of radial distribution functions are considered.

APPENDIX II. Effects of the Asymmetry of Strands

We have assumed that the strands composing fibrous systems have cylindrical symmetry. Eq.(A1) and Eq.(A2) is derived under this assumption. Actually, there must be some deviations from the cylindrical symmetry in the structure of the strands. In this Appendix, the effects of the asymmetry of the strands on the radial distribution function are discussed. The theoretical treatment of the asymmetry is difficult. So, in order to investigate the effects of the asymmetry, the strands are considered to be composed from two sub-strands, which have cylindrical symmetry. The sub-strands are separated with the distinct distance, δ, with each other (splitting atom approximation). Then, the intensity formula are rewritten,

$$I(R) = 2Nf'^{2}(R)\left[1 + \frac{1}{2N}\sum_{k,l}\sum_{i,j} J_o(2\pi R r_{ijkl})\right] \qquad (A7)$$

$$i(R) = 1 + \frac{1}{2N}\sum_{k,l}\sum_{i,j} J_o(2\pi R r_{ijkl}) \qquad (A8)$$

Here, $f'^{2}(R)$ is the scattering intensity of the sub-strands. The suffix (i,j) is refered to the strands and the suffix (k,l) is refered to the sub-strands in a strand. If the splitting distance, δ, is small, Eq.(A7) can be rewritten for small R,

$$I(R) \approx N\left\{2f'^{2}(R)\left[1+J_o(2\pi R\delta)\right]\right\}\left\{1+\frac{2J_o(2\pi R\bar{\delta})}{1+J_o(2\pi R\delta)}\cdot\frac{1}{N}\sum_{i\neq j} J_o(2\pi R\bar{r}_{ij})\right\} \qquad (A9)$$

$$\approx N\left\{2f'^{2}(R)\left[1+J_o(2\pi R\delta)\right]\right\}\left\{1+\frac{1}{N}\sum_{i\neq j} J_o(2\pi R\bar{r}_{ij})\right\} \qquad (A10)$$

Here, $\bar{\delta}$, is the mean distance of the order of δ and $\bar{r}_{ij}$ is the distance between the centres of strands. The mean distance, $\bar{\delta}$, is dependent on the mutual orientation of asymmetric strands. Eq.(A9) and (A10) show that the asymmetry of the strands is negligible at small R and the molecular scattering intensity of a strand becomes to cylindrical one, $2f'^{2}(R)(1+J_o(2\pi R\delta))$. And Eq.(A9) also shows that the another damping factor for the oscillation of $J_o(2\pi R\bar{r}_{ij})$, that is, $2J_o(2\pi R\bar{\delta})/(1+J_o(2\pi R\delta))$, which depends on the mutual orientation. Strictly speaking, this is not simple decay function as Gaussian, but damping oscillation function due to mainly $J_o(2\pi R\bar{\delta})$.

In Fig.A4, the structural model is shown for the case of two asymmetric strands, which contain two sub-strands with the splitting distance of one tenth of the inter-strands distance, $\delta=\frac{a}{10}$. The interference function can be calculated according to Eq.(A8) if the mutual orientation is given. Fig.A4 also shows the interference function from the model cited in the figure. The interference function of sub-strands themselves, $1+J_o(2\pi R\delta)$ is also shown. The interference function with splitting are oscillating around the interference function of splitting itself, as mentioned above. This is true for other two dimensional arrays of more elements with splitting, if the splitting is rather small compared to the inter-strand distance. The additional damping of the oscillation can be seen in Fig.A4, which is dependent on the mutual orientation, as

mentioned above.

Thus, when the fibrous systems are composed from asymmetric strands, the empirical method will give the similar interference function for the disposition of the centres of strands for the region, $R \ll 1/\delta$. Only, the damping oscillation is faster than the case of the symmetric strands. The errors introduced to radial distribution functions by the empirical method were examined by model calculations. These are shown in Fig.A5, for examples. (a) is the obtained radial distribution function of the annular array of 6 strands with splitting, $\delta=a/10$ and (b) is of 11 strands with same splitting. The true positions corresponding to the distances between the centres of strands are shown with arrows. And the positions of the peaks corresponding to sub-strands are also shown on the base line. The integration of the Fourier-Bessel transformation of Eq.(A4) was carried out in the region, $R \lesssim 1/\delta$. As a result of many systematic calculations for other cases, it is to say that the each peak of the modified radial distribution function becomes broad but the clearly observed peaks well correspond to the peaks of the distances between centres of strands (arrowed position). Beside the clearly observed peaks, several sub-peaks are observed, but some of these sub-peaks are quite artificial. When the splitting separation of sub-strands becomes large, the radial distribution functions become complex and do not give simple peaks. However, when

the first clearly observed peak corresponding to the nearest neighbour distance is not splitted, other peaks which correspond to the distances between centres of strands are also clearly observed. And the correspondence between clearly observed peaks and the peaks of the centre-to-centre distances is good. The artificial sub-peaks may be originated from $2J_o(2\pi R\bar{\delta})/(1+J_o(2\pi R\delta))$. This additional factor is not simple decay function, as mentioned above. Then, the interference functions obtained by the empirical method have not the simple damping oscillations.

Conclusively it may be said that the small asymmetry of the strands causes to broadening of the peaks of radial distribution function. And the empirical method are available, so long as the first main peak of the obtained radial distribution function is not separated, since in these cases the correspondence is sufficient as mentioned above.

References

1. T. Iino, Bact. Rev., 33 (1969) 454.
2. D. J. Kushner, Bact. Rev., 33 (1969) 302.
3. S. Asakura, Adv. Biophys., 1 (1970) 99.
4. Y. Uratani, S. Asakura and K. Imahori, J. Mol. Biol., 67 (1972) 85.
5. S. Fujime, M. Maruyama and S. Asakura, J. Mol. Biol., 68 (1972) 347.
6. B. R. Gerber, L. M. Routledge and S. Takashima, J. Mol. Biol., 71 (1972) 317.
7. D. Abram, H. Koffler and A. E. Vatter, J. Bacteriol., 90 (1965) 1337.
8. D. Kerridge, W. R. Horne and A. M. Glauert, J. Mol. Biol., 4 (1962) 227.
9. J. Lowy and J. Hanson, J. Mol. Biol., 11 (1965) 293.
10. J. N. Champness and J. Lowy, Proc. Symposium on Fibrous Proteins, ed. W. G. Crewther, Butterworth and Company, Australia, 1968, p.106.
11. J. N. Champness, J. Mol. Biol., 56 (1971) 295.
12. K. Wakabayashi and T. Mitsui, J. Mol. Biol., 53 (1970) 567.
13. J. Lowy and J. Spencer, Symp. Soc. Exptl. Biol., 22 (1968) 215.
14. U. B. Sleytr and A. M. Glauert, Nature (London), 241 (1973) 542.
15. E. J. O'Brien and P. N. Bennett, J. Mol. Biol., 70 (1972) 133.

16. J. T. Finch, Fifth Eur. Cong. Electron Microscopy, Manchester, 1972.

17. J. T. Finch and A. Klug, Sohn Innes Symp., Norwich, 1972.

18. G. Swanbeck and B. Forslind, Biochim. Biophys. Acta, 88 (1964) 422.

19. W. Bode, J. Engel and D. Winklmair, Eur. J. Biochem., 26 (1972) 315.

20. G. Oster and D. P. Riley, Acta Cryst., 5 (1952) 272.

21. R. E. Burge, Acta Cryst., 12 (1959) 285.

22. R. E. Burge, Proc. Roy. Soc. A, 260 (1961) 558.

23. R. E. Burge, J. Mol. Biol., 7 (1963) 213.

24. R. E. Franklin and K. C. Holmes, Acta Cryst., 11 (1958) 213.

25. B. A. Fedorov, Acta Cryst., A27 (1971) 35.

26. T. Iino, Genetics, 46 (1961) 1465.

27. S. Asakura, G. Eguchi, and T. Iino, J. Mol. Biol., 10 (1964) 42.

28. S. Asakura, G. Eguchi, and T. Iino, J. Mol. Biol., 16 (1966) 302.

29. T. Yamaguchi, M. Hayashi, K. Wakabayashi and S. Higashi-Fujime, Biochim. Biophys. Acta, 257 (1972) 30.

30. K. Wakabayashi, T. Yamaguchi and H. Kagawa, J. Mol. Biol., in press.

31. A. Elliott, J. Sci. Instr., 42 (1965) 312.

32. P. W. Schmidt and R. Hight, Acta Cryst., 13 (1960) 480.

33. B. K. Vainshtein, Diffraction of X-rays by Chain Molecules, Elsevier, Amsterdam, 1966.

34. A. Guinier, X-ray Diffraction in Crystals, Imperfect Crystals and Amorphous Bodies, Freemen, San Fransisco, 1963.

35. A. N. J. Heyn, J. Appl. Phys., 26 (1955) 1113.

36. U. W. Arndt and D. P. Riley, Philos. Trans., 247 (1955) 409.

37. R. D. B. Fraser, T. P. MacRae and A. Miller, J. Mol. Biol., 14 (1965) 432.

38. J. D. Bernal and C. H. Carlisle, Acta Cryst., 12 (1959) 221.

39. G. N. Watson, A Treatise on the Theory of Bessel Functions, Cambridge University Press, Cambridge, 2nd ed., 1958.

40. O. Kratky and G. Porad, Acta Physica Austriaca, 2 (1948) 133.

41. A. Guinier and G. Fournet, Small-Angle Scattering of X-rays, Wiley and Sons, New York, 1955.

42. R. E. Burge and J. C. Draper, J. Mol. Biol., 56 (1971) 21.

43. H. Lipson and W. Cochran, The Determination of Crystal Structures, G. Bell and Sons, London, 1966.

44. K. Wakabayashi, private communication.

45. K. Furuya, private communication.

Table 1

Spacings (Å) of X-ray reflections from Salmonella flagella

Solution	Fibre (Equatorial)
(44.4)	
	40.2
28.2	27.8
(25.9)	
(22.7)	
20.0	21.2
15.6	15.1
12.9	12.6
(11.5)	11.0
10.4	
9.45	9.41
8.56	8.35
7.77	7.47
(7.28)	
6.33	6.58
(5.82)	5.95
	5.37

Figure Captions

Fig.1 Models of bacterial flagella. (a) Eight longitudinal strands of spherical subunits close-packed on the surface of a cylinder, presented by Lowy and Hanson.[9] (b) Modified Lowy-Hanson model built from wedge-shaped sub-units, presented by Bode et al..[19]

Fig.2 Flow chart for preparation of Salmonella flagella.

Fig.3 Flow chart of depolymerization-polymerization process for purification of flagella.

Fig.4 The slit-corrected small-angle equatorial X-ray scattering curve for Salmonella flagella. The concentration of the solution is 12 mg protein/ml. The ordinate is the corrected intensity, that is, intensity times scattering angle.

Fig.5 Moderate-angle equatorial X-ray diffraction intensities of flagella. (———) Data from oriented fibre specimens; (—— – ——) from aqueous solution specimens, concentration of 24 mg protein/ml.

Fig.6 Guinier plot of the small-angle equatorial scattering curve of flagella. The concentration is 6 mg protein/ml. The ordinate indicates the

observed intensity times scattering angle. The full line corresponds to the radius of gyration of the cross-section of 68 Å.

Fig.7 Cylindrically averaged electron density distribution of Salmonella flagella, obtained by the Fourier-Bessel transformation method. (———) the phase combination of (+,-,-) for the principal peak at the origin and two subsidary peaks; (— – —) the phase combination of (+,-,+).

Fig.8 The molecular scattering intensity of the strands in Salmonella flagella (— – —). The full line is the observed equatorial diffraction intensity. Molecular scattering intensity was obtained by averaging two smooth curves, shown as dotted lines.

Fig.9 The interference function for the arrangement of the strands in Salmonella flagella. The interference function is obtained by dividing diffraction intensity shown in Fig.5 by the molecular scattering intensity of Fig.9.

Fig.10 The damping profile of the interference function of Fig.9. The full line corresponds to the equivalent standard deviation of 3 Å.

Fig.11 The radial distribution function of the arrangement of the strands in Salmonella flagella. This is obtained from the interference function of Fig.10 by the Fourier-Bessel transformation. The Fourier-Bessel transformation is carried out against i(R)-1.

Fig.12 Calculated radial distribution function for annular arrays. The calculation is achieved under the fixed nearest neighbour distance at 35.5 Å. The abscissa is the number of the strands of annular models. Circles indicate the positions of the peaks of the calculated radial distribution functions and horizontal full lines and dashed lines indicate the positions of clear peaks of Fig.11 and the breadth for each peaks.

Fig.13 Comparison between calculated diffraction intensities and observed one. The calculated intensities are indicated the models of 8, 11, and 13 strands which are annularly arranged with the nearest neighbour distance of 35.5 Å. These are calculated using the molecular scattering intensity of Fig.8 and the equivalent standard deviation of 4 Å.

Fig.14 The discrepancy factors for annular models. The abscissa is the number of the strands of the

annular models. The discrepancy factors are calculated for the interference function shown in Fig.9.

Fig.15 Calculated diffraction intensity for the 11 strands model. The equivalent standard deviation is considered as 3 Å. (———) calculated intensity; (— – —) observed intensity.

Fig.16 An example of a drawing of the 11 strands model. The helical symmetry of this diagram is that of 2 turns and 11 residues helix. The surface lattice is that a=46 Å, b=51.9 Å and r=128°. Assuming the spherical sub-units, there appear considerable vacant spaces between subunits.

Fig.17 Top views of the 11 strands model shown in Fig.16. In the figure, the average radius $\bar{r}$ and the inner and outer radii r_1 and r_2 are also indicated. The dotted line is the cylindrically averaged electron density shown in Fig.7 as (———).

Figure Captions of Appendices

Fig.A1 Interference functions for the two dimensional arrays of 6 strands shown in the figure.

Fig.A2 Errorneous interference functions for the annular array of 6 strands. (— + —) u_o=12, A=1/144; (——·——) u_o=12, A=10/144. The full line is the true interference function.

Fig.A3 Radial distribution functions obtained from the errorneous interference functions of Fig.A2.

Fig.A4 Interference function of the system of two splitted strands. The splitting distance is one tenth of the nearest neighbour distance between the centres of the strands. Mutual orientation of the strands is shown in the figure.

Fig.A5 Radial distribution functions obtained by the empirical method for annular arrays of splitted strands. The upper one is for the annular array with 6 splitted strands and the lower one is for 11 splitted strands.

Plate Captions

Plate 1 Flagella of Salmonella strain SJ25, an electron micrograph of reconstituted normal flagella used in this studies. Flagella are negatively stained with 1 % uranyl acetate (pH about 4.5). × 340.000.

Plate 2 Moderate-angle X-ray diffraction patterns of Salmonella flagella. (a) oriented fibre specimens, effective camera length of 12.3 cm. (b) aqueous solution specimens, effective camera length of 12.3 cm.

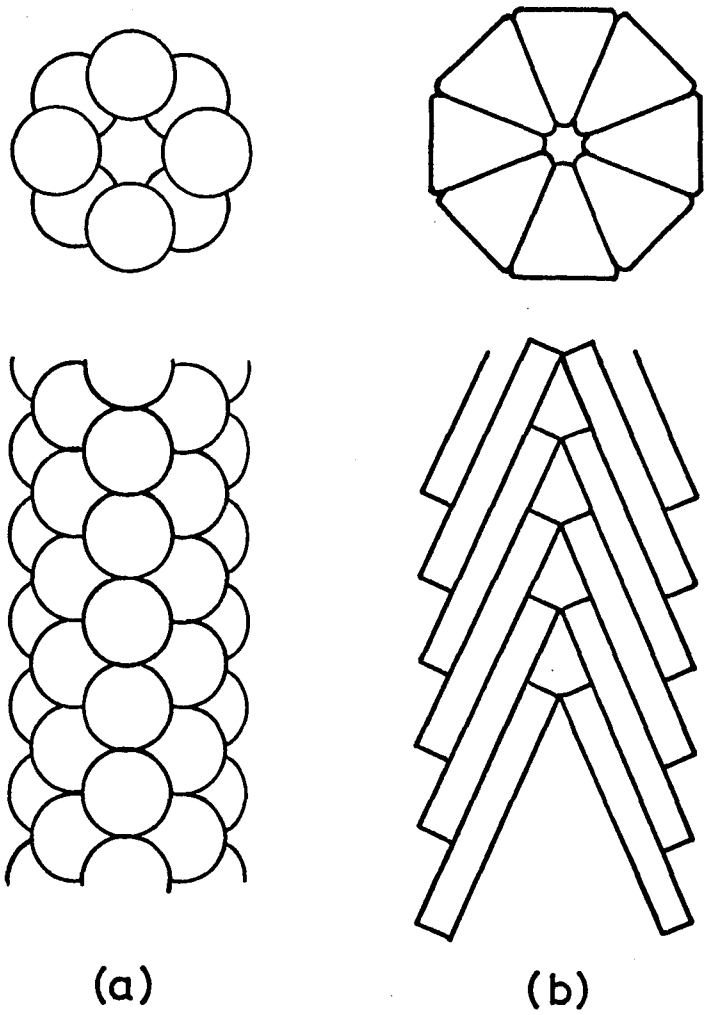

Fig. 1

Fig. 2

PREPARATION OF FLAGELLA OF SALMONELLA SJ25

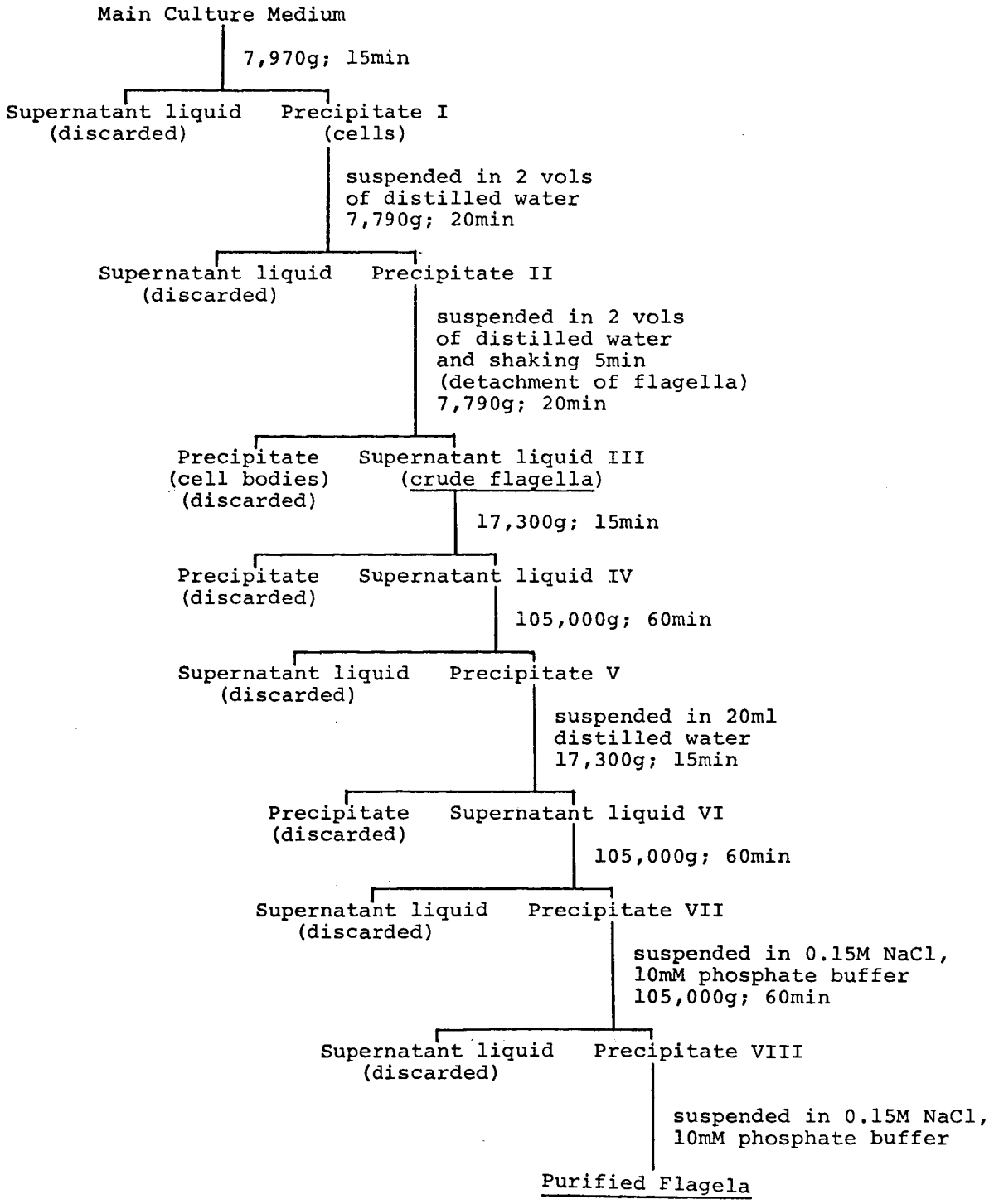

Fig. 3

PURIFICATION OF FLAGELLA

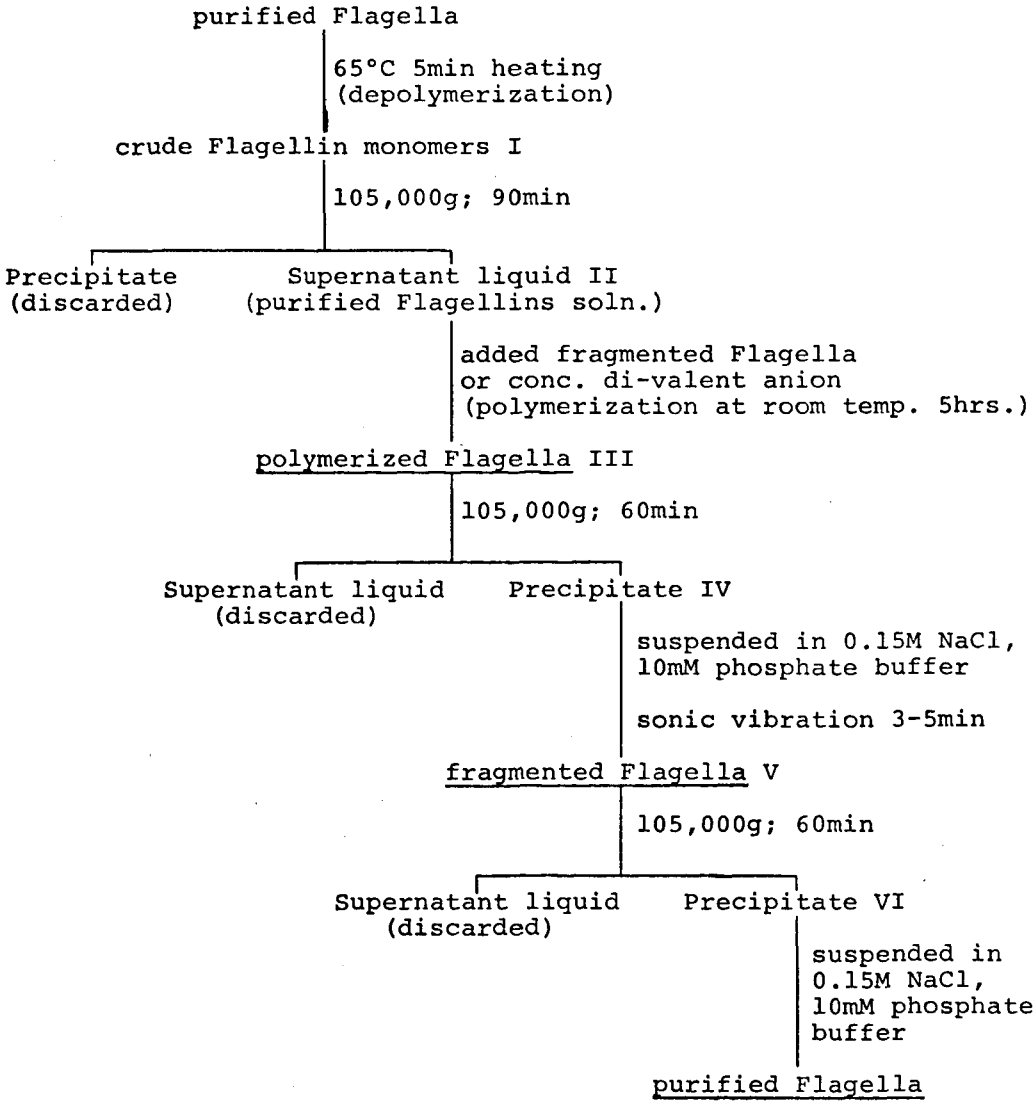

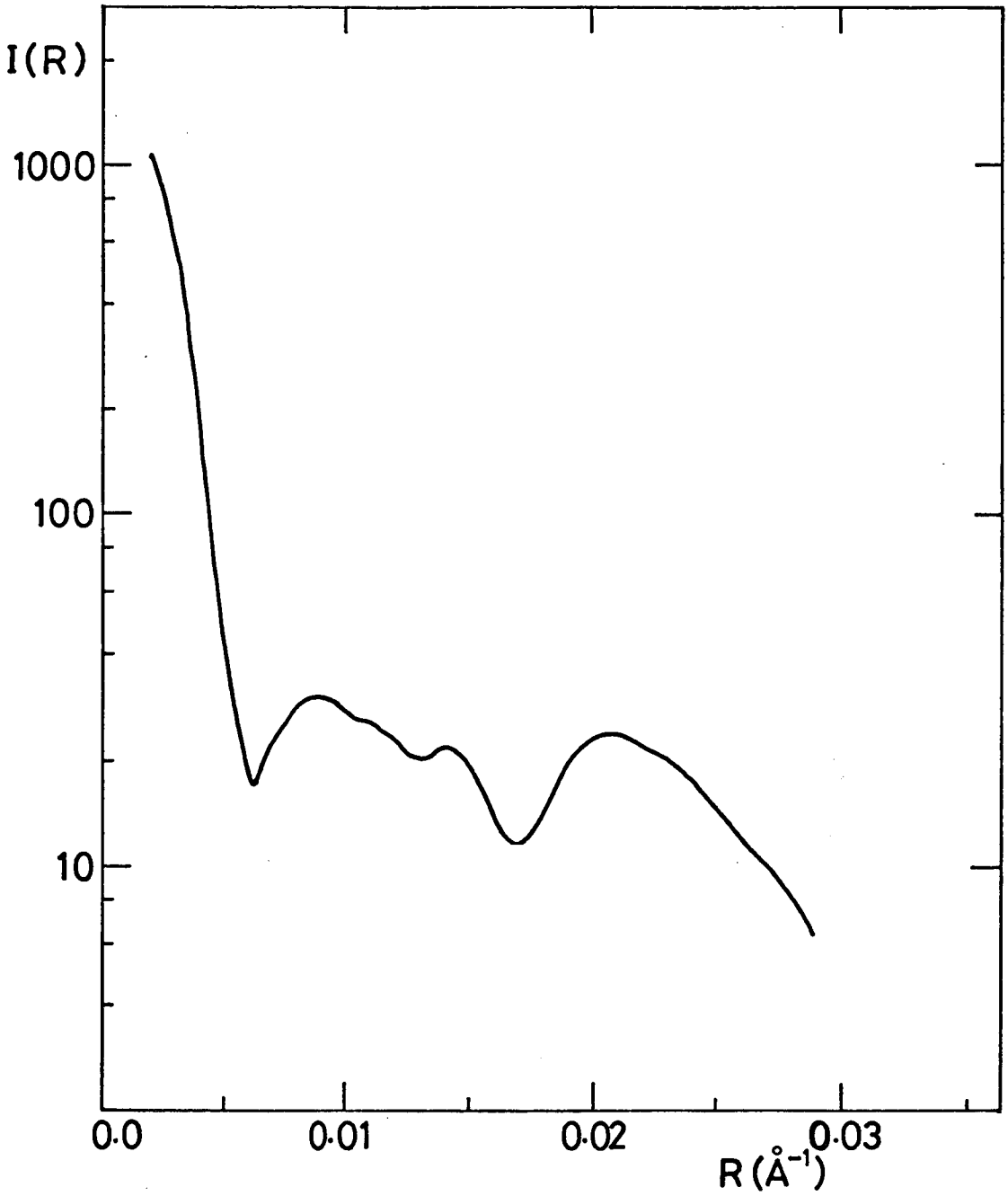

Fig.4

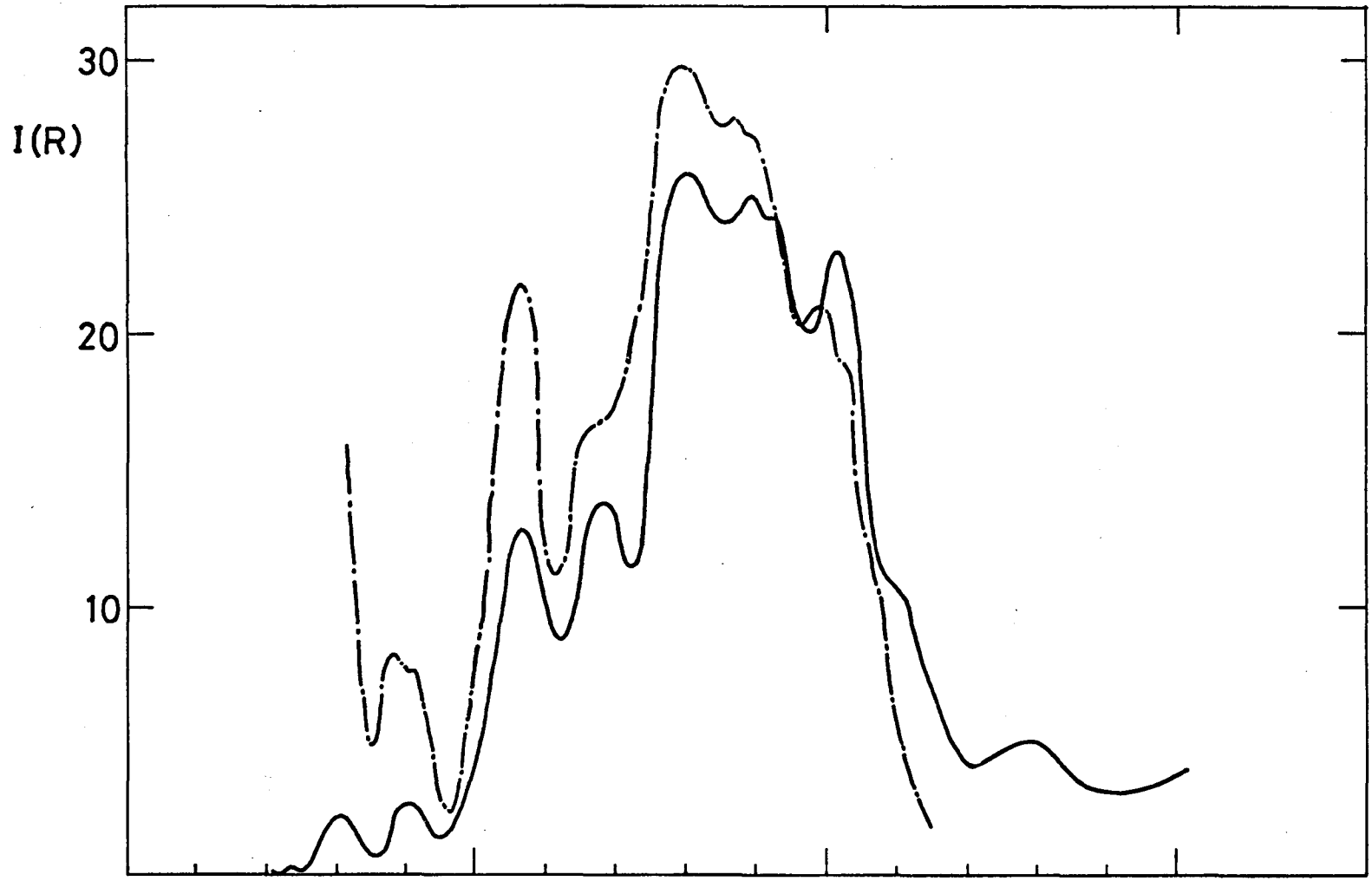

Fig. 5

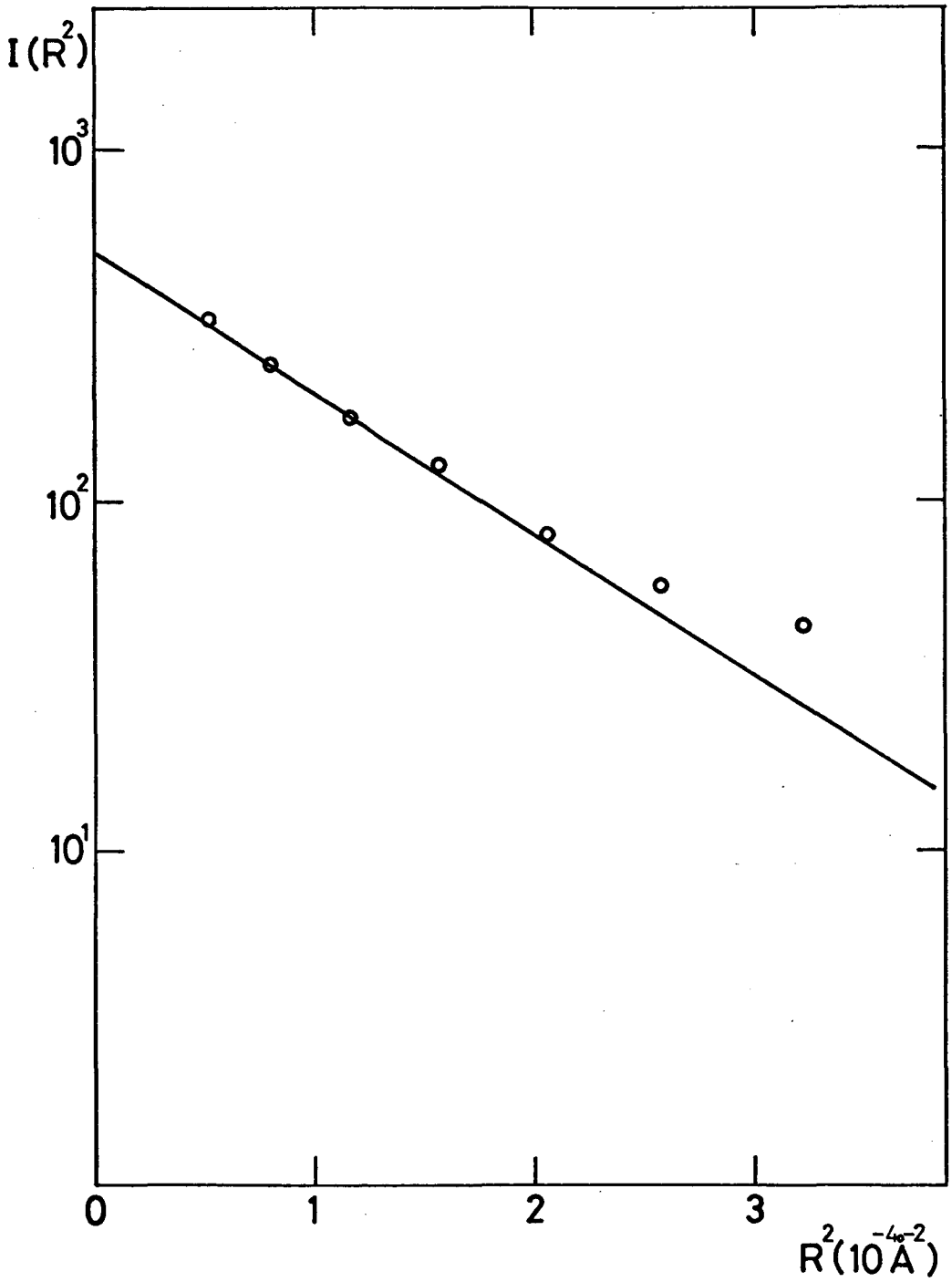

Fig. 6

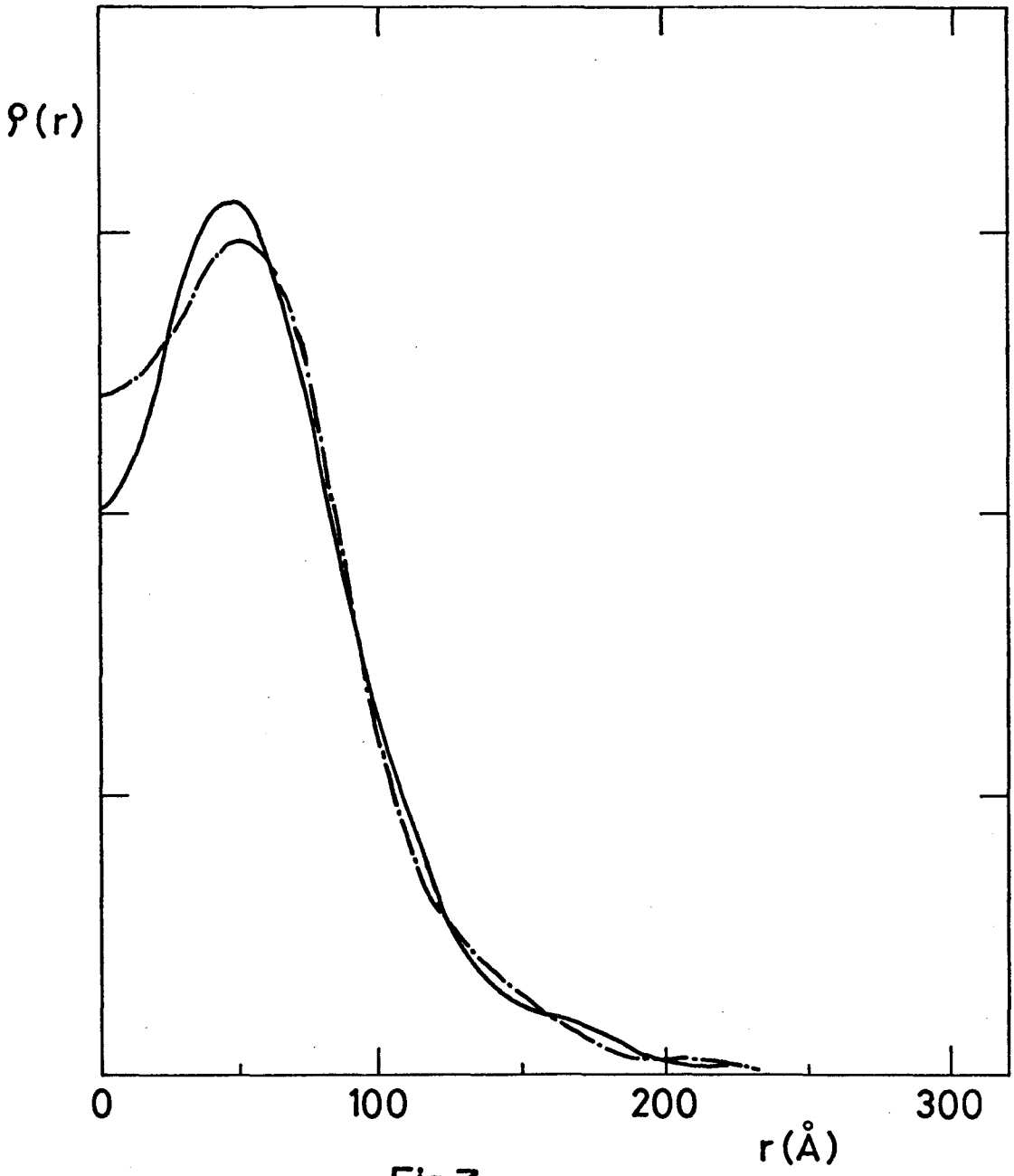

Fig.7

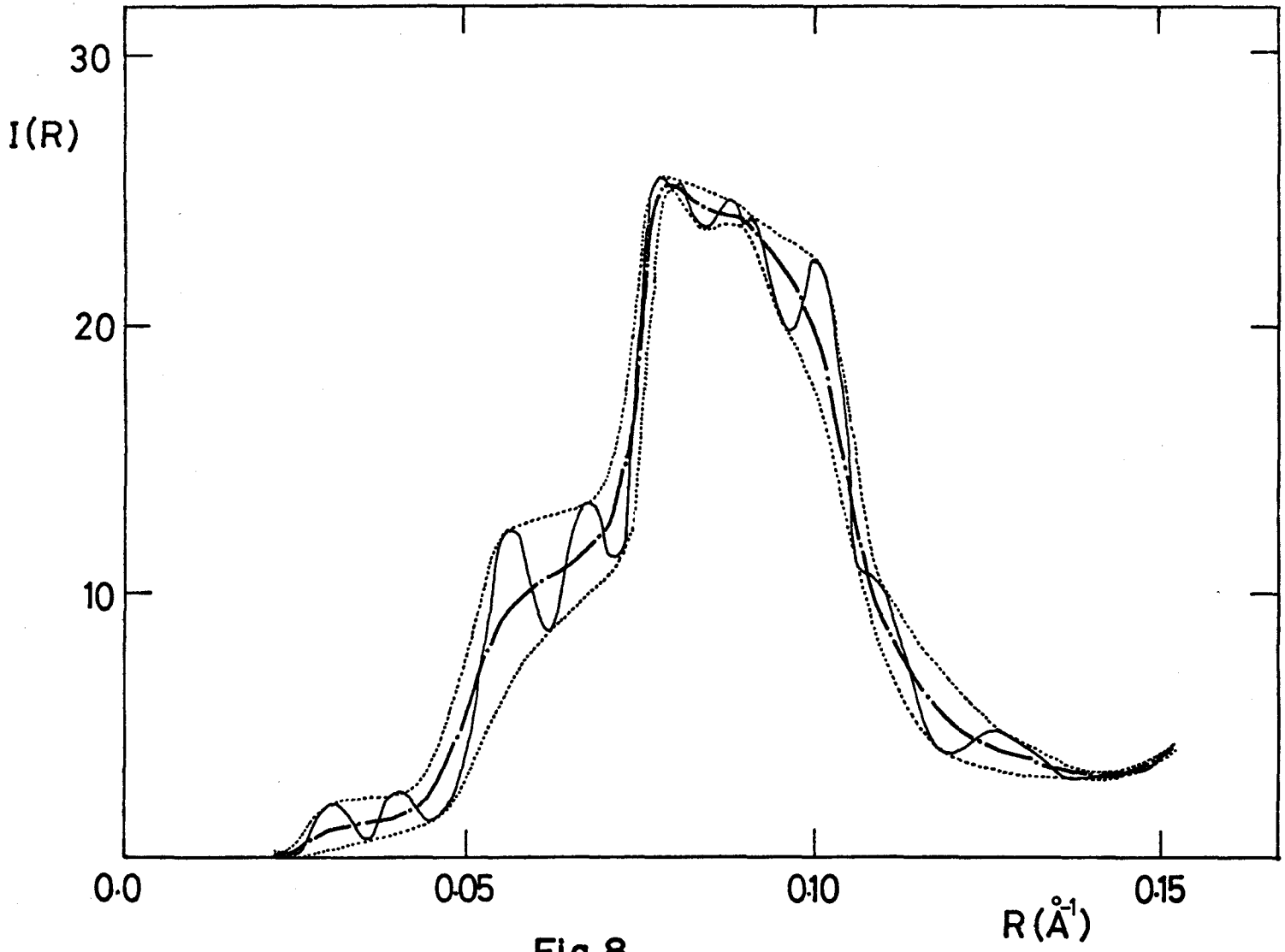

Fig. 8

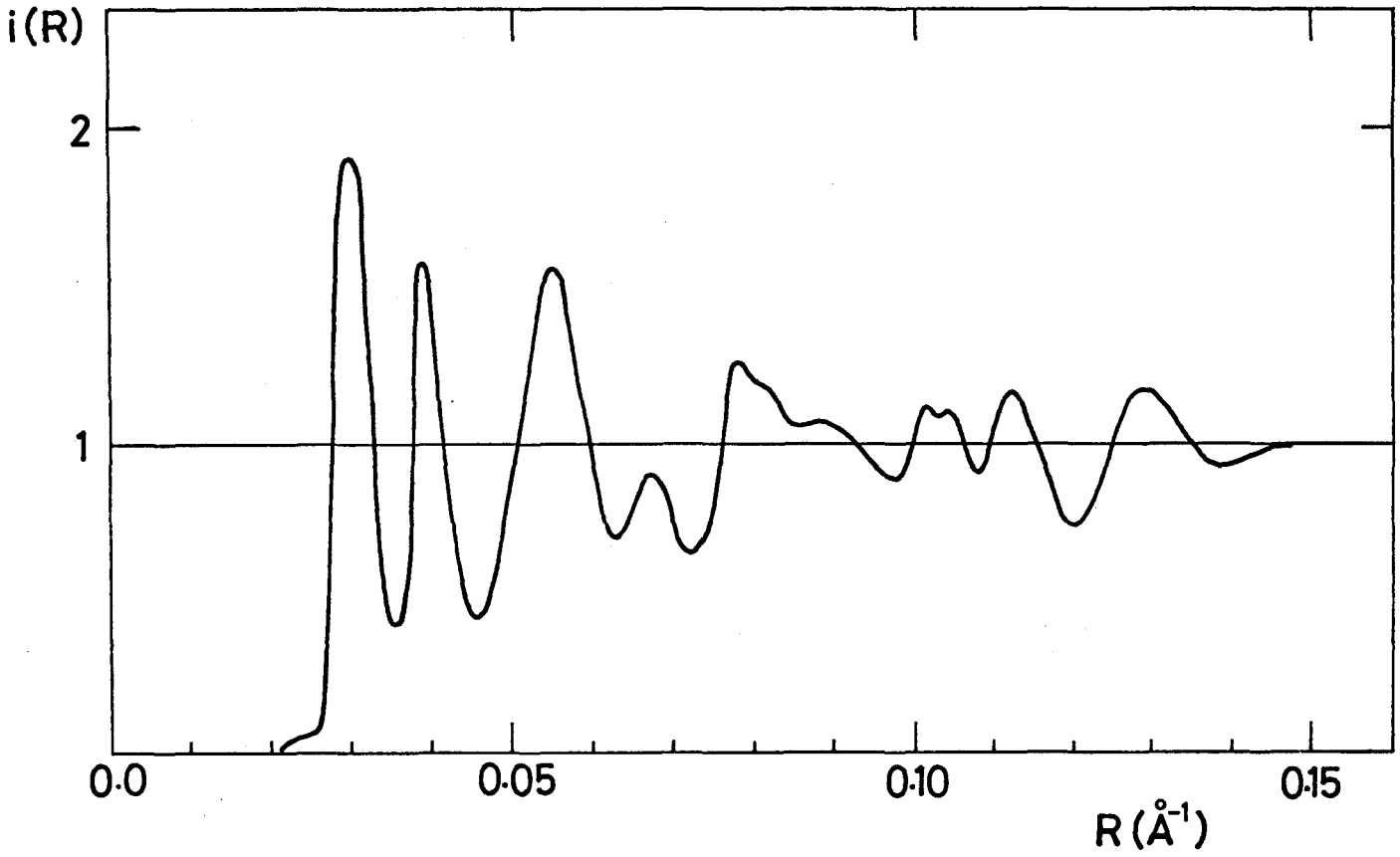

Fig.9

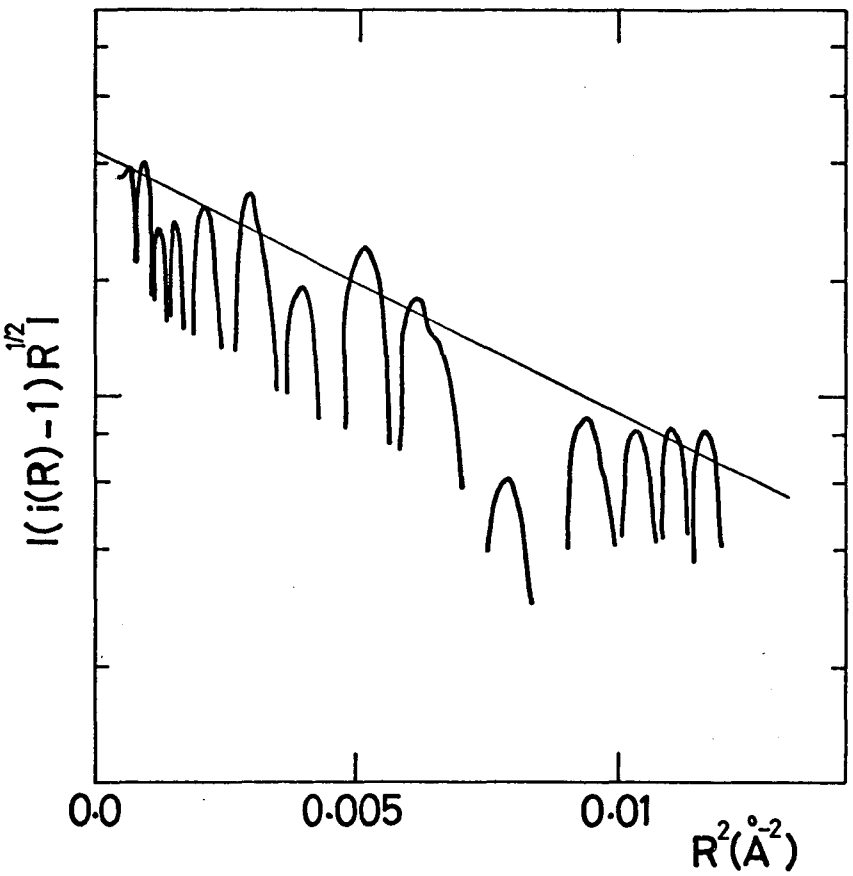

Fig. 10

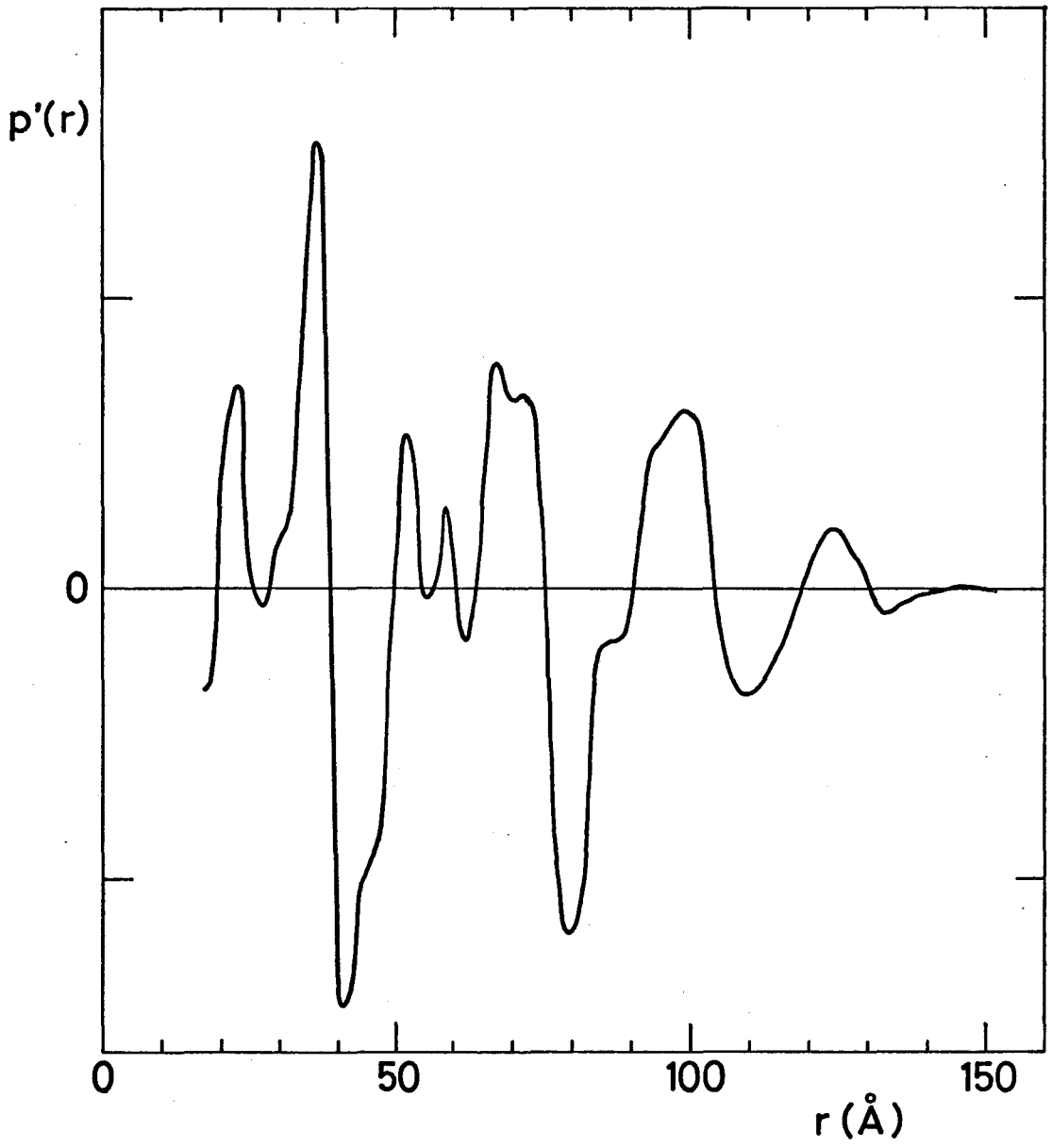

Fig. 11

Fig. 12

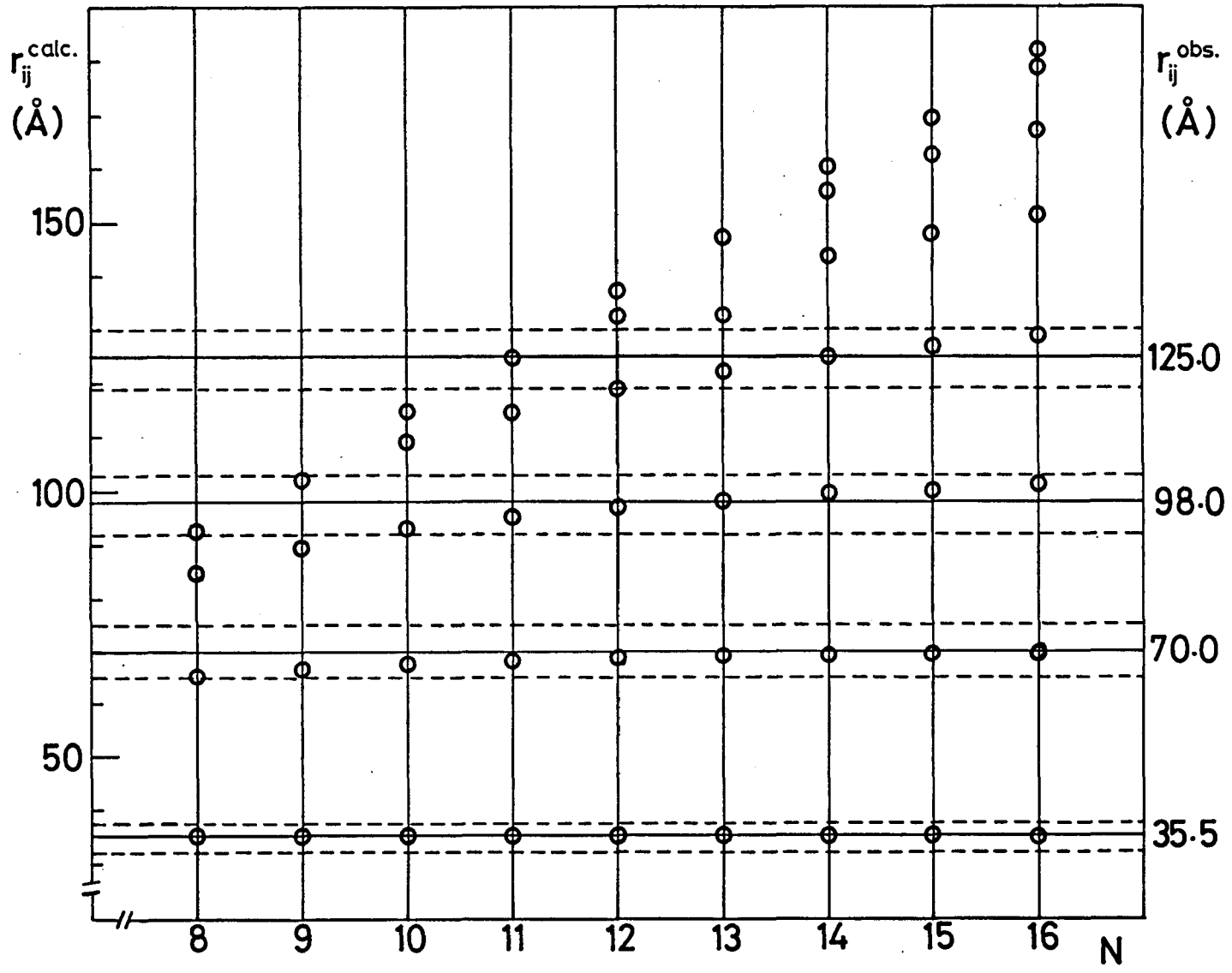
$r_{ij}^{calc.}$ (Å)
150
100
50
8
9
10
11
12
13
14
15
16
N
$r_{ij}^{obs.}$ (Å)
125·0
98·0
70·0
35·5

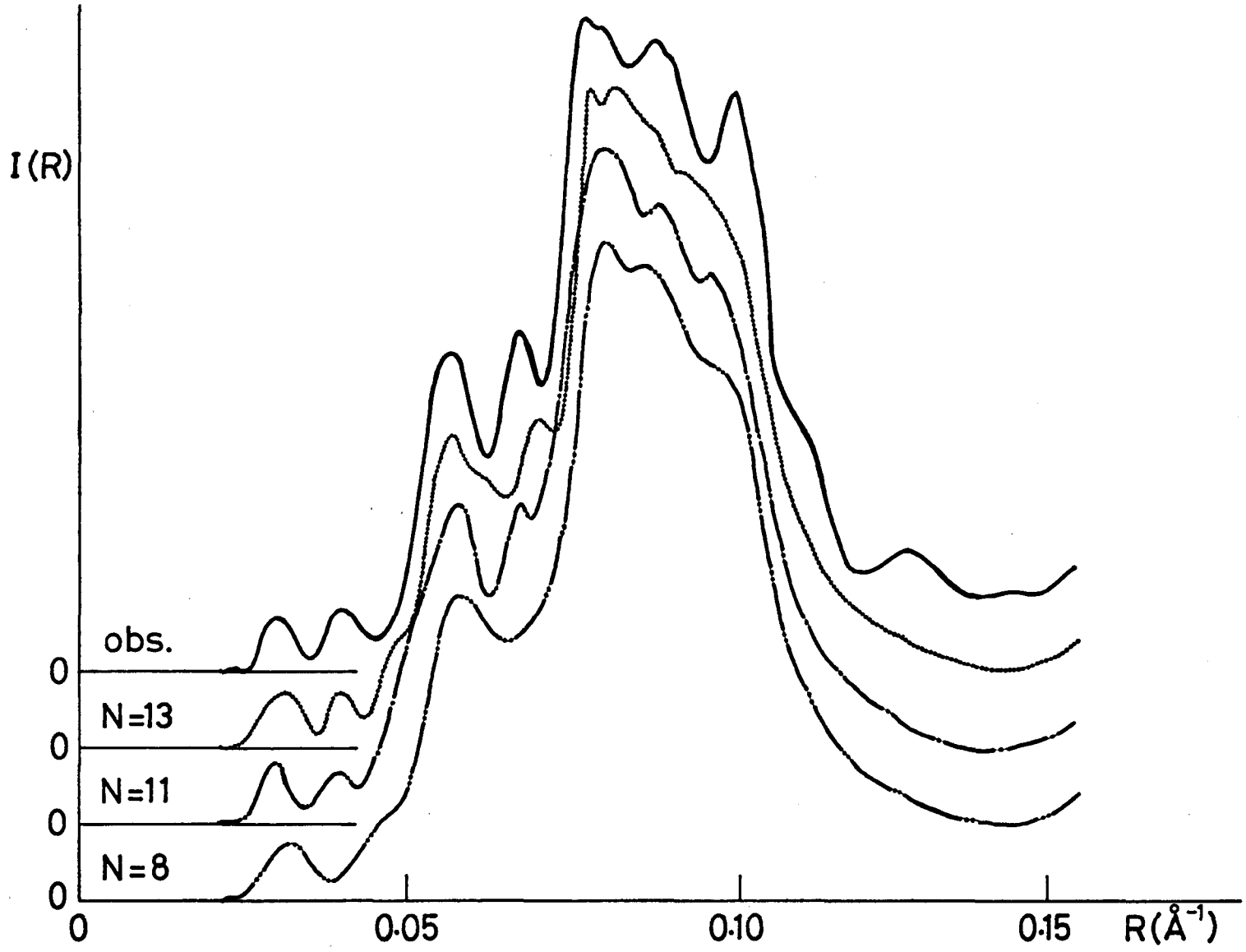

Fig.13

Fig.14

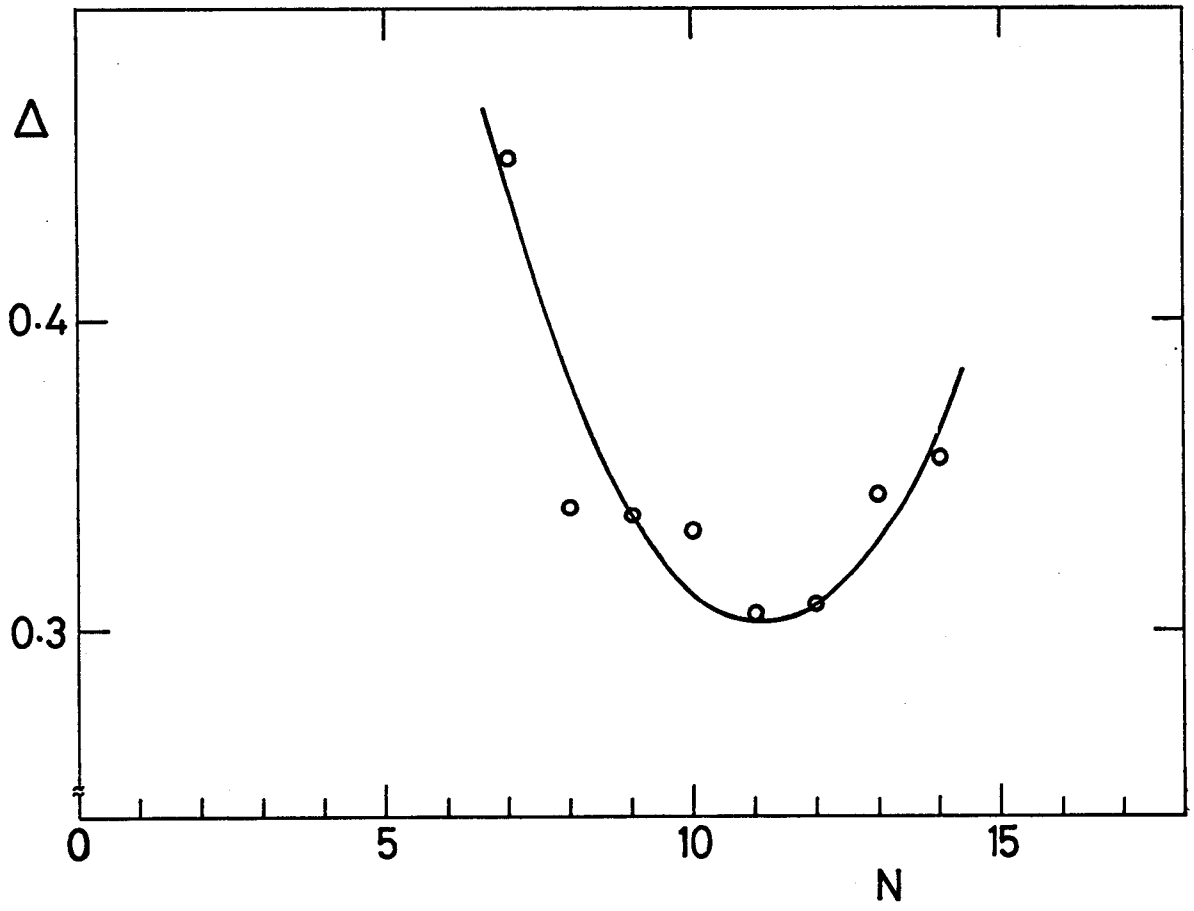

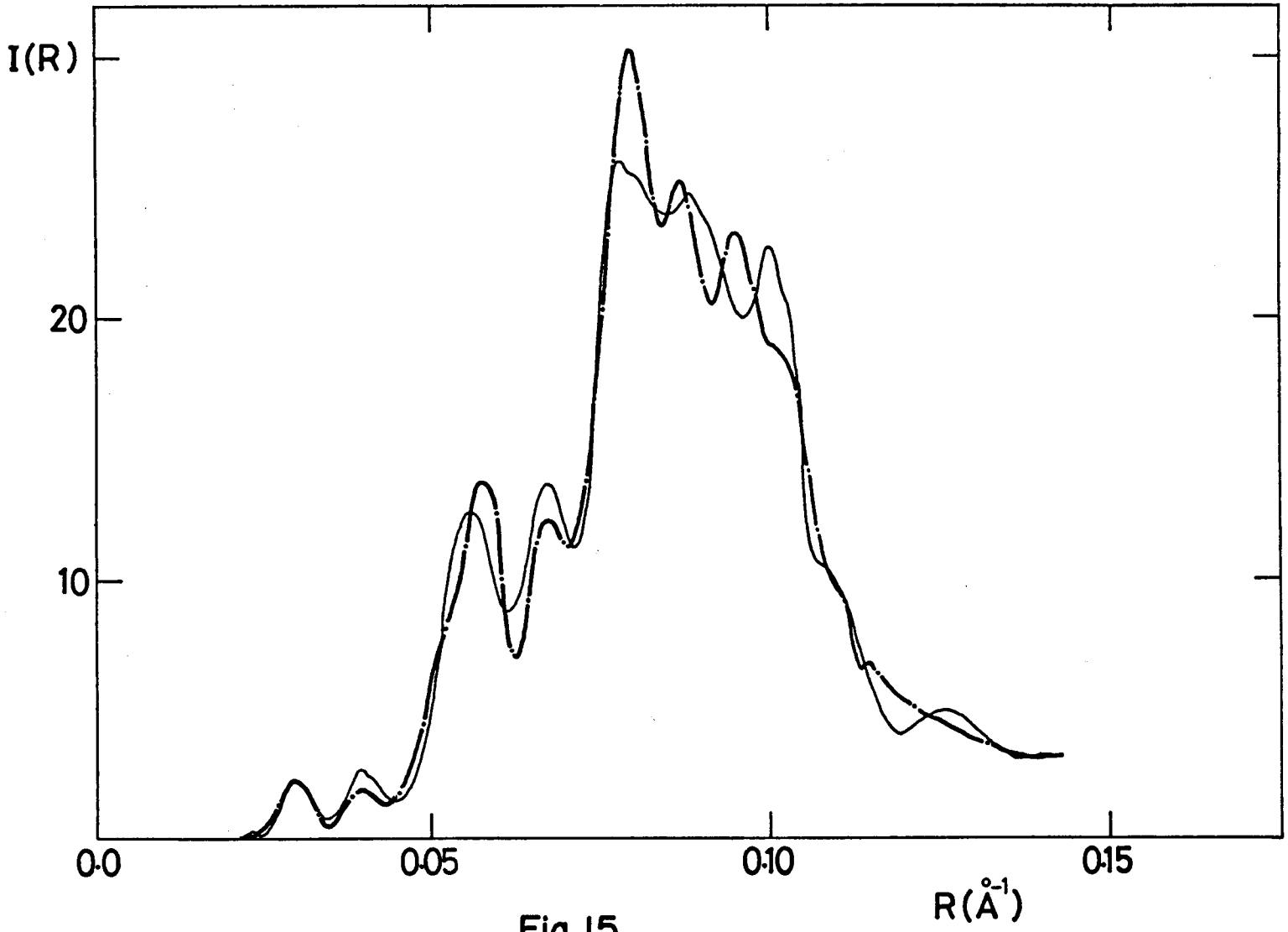

Fig.15

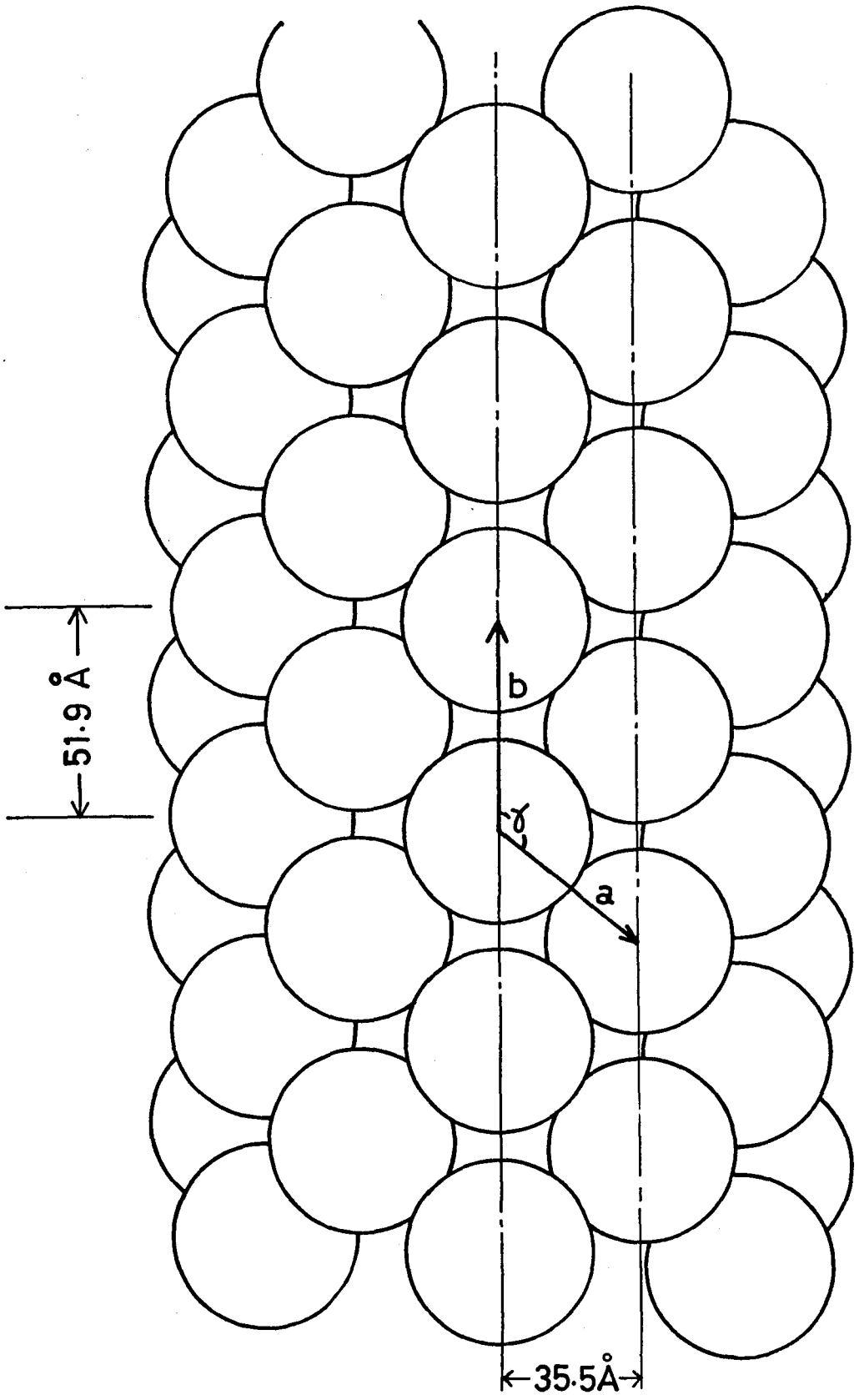

Fig.16

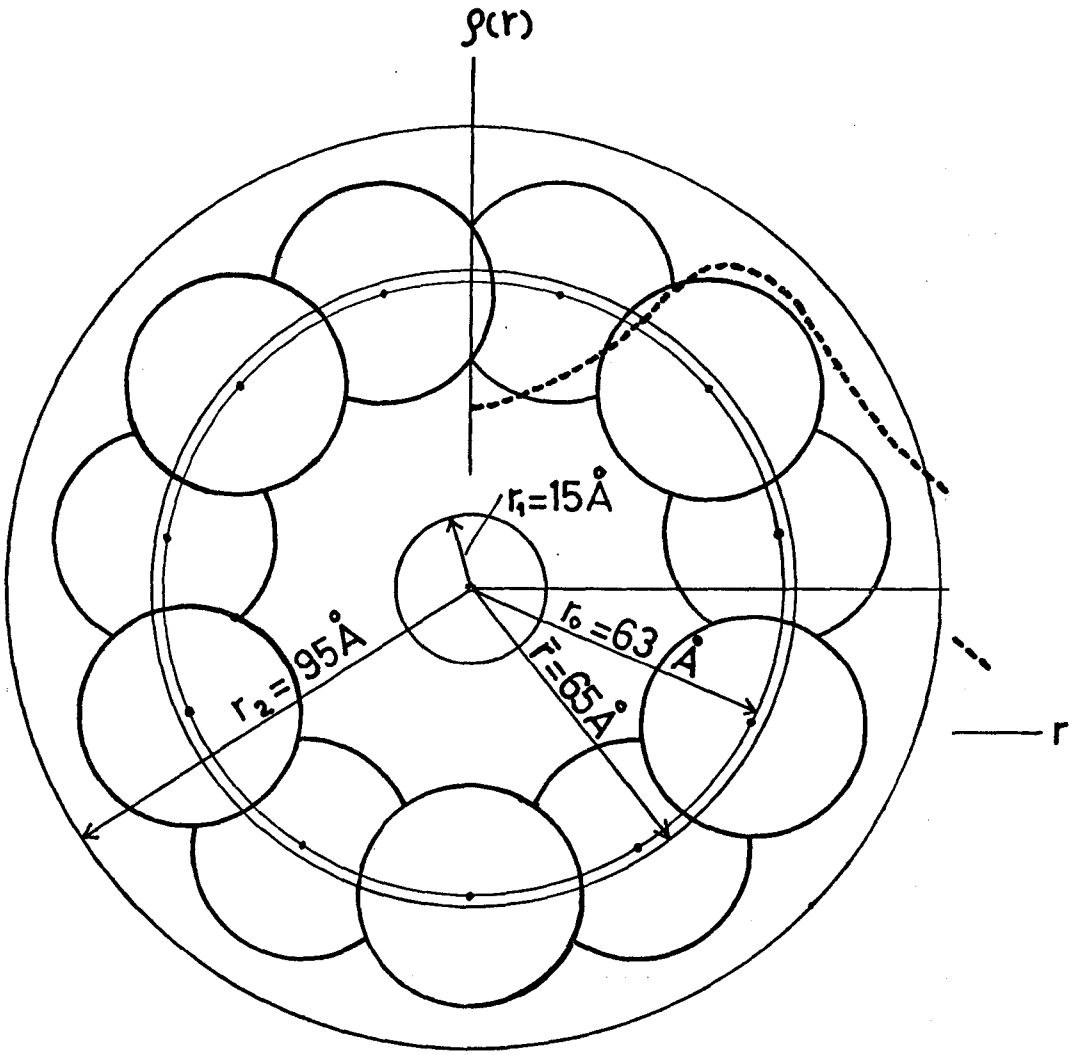

Fig. 17

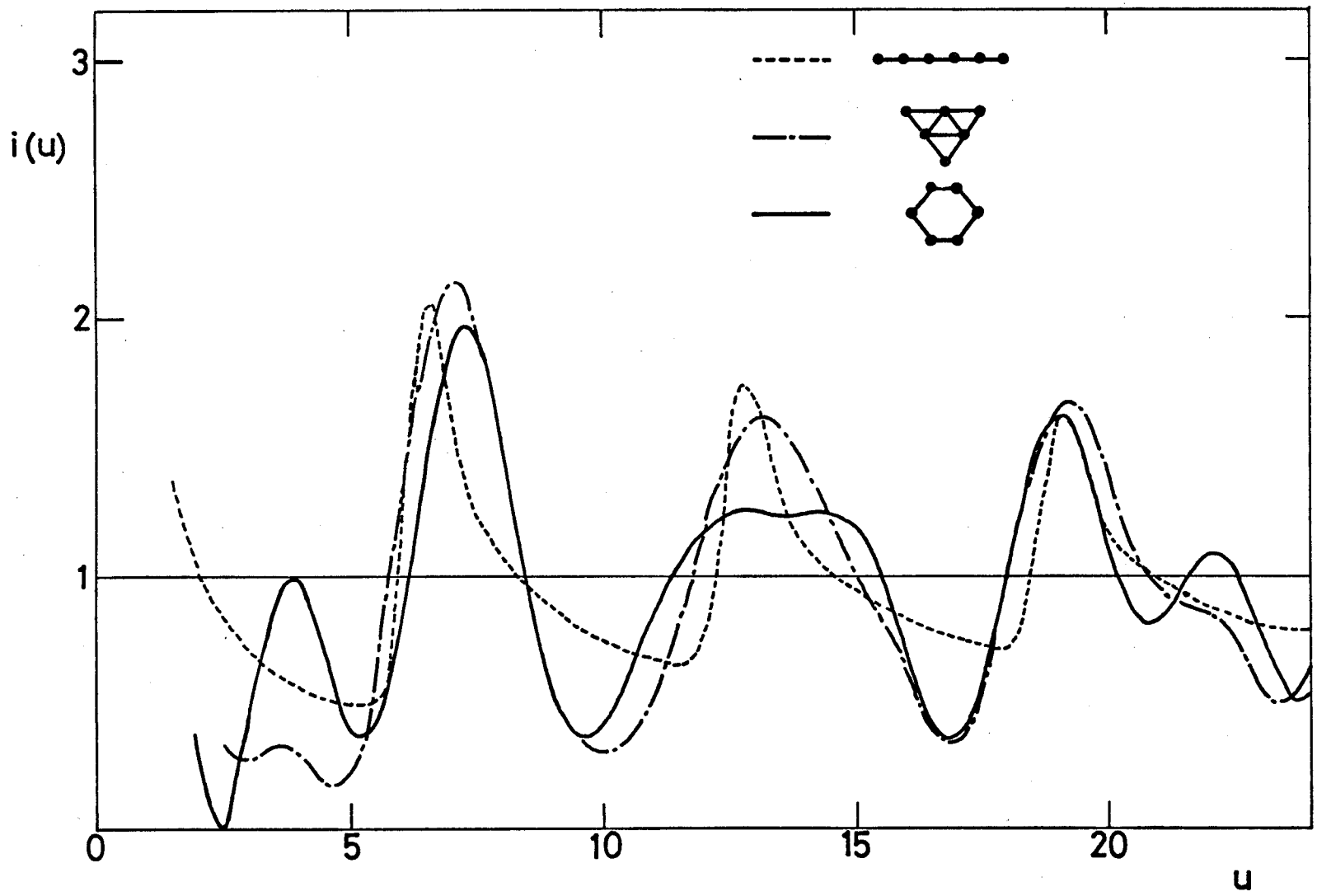

Fig. AI

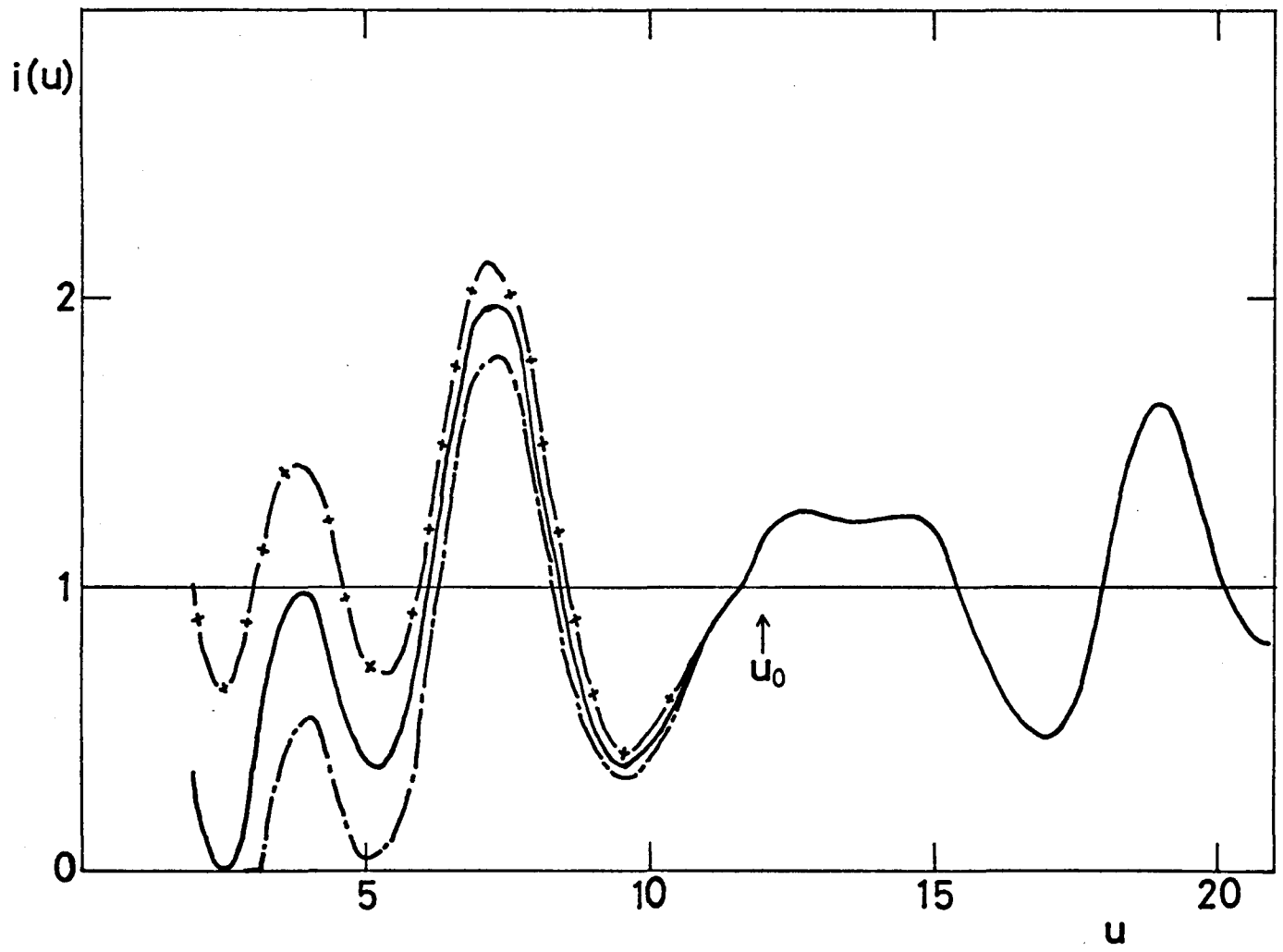

Fig.A2

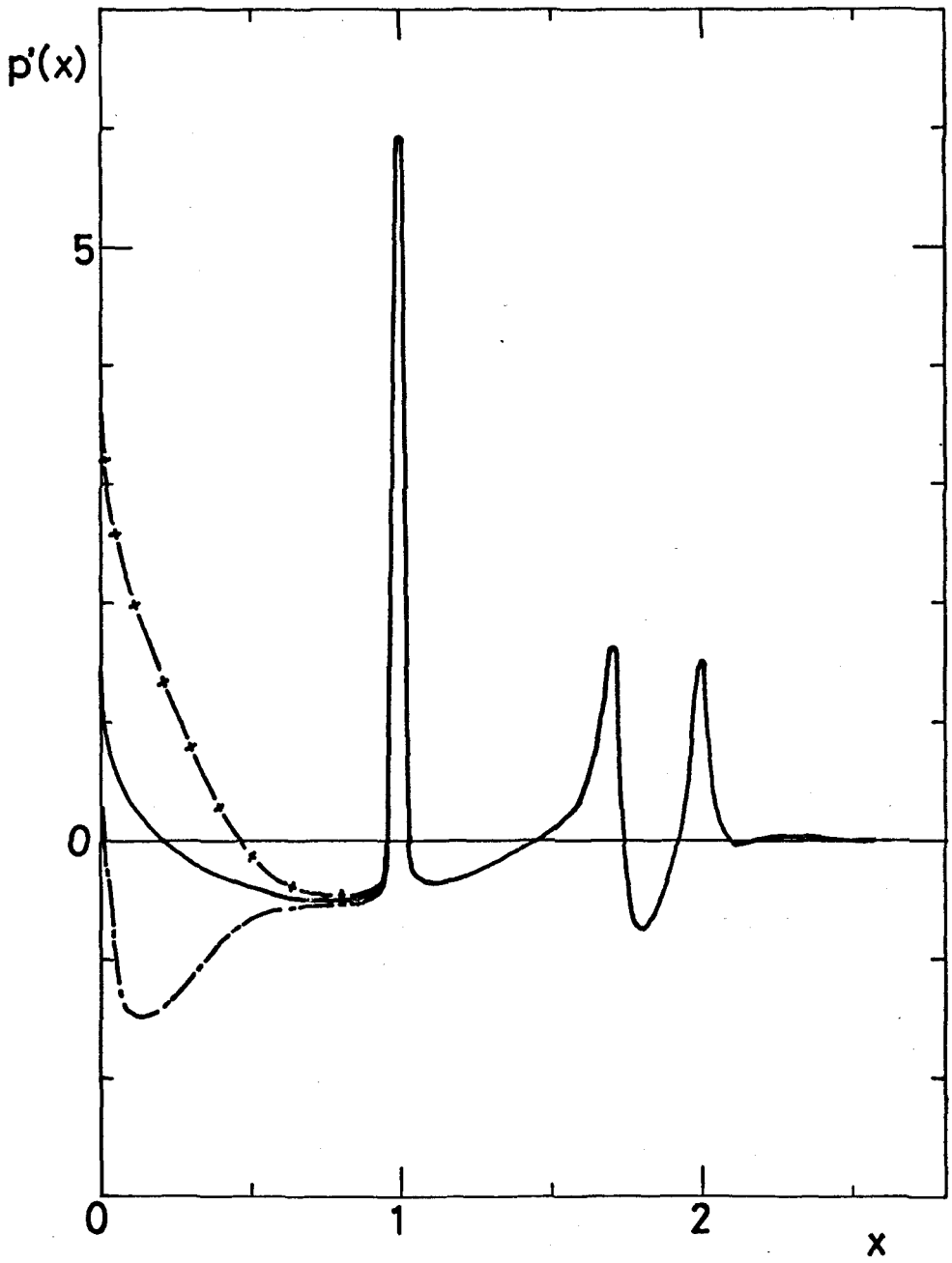

Fig. A3

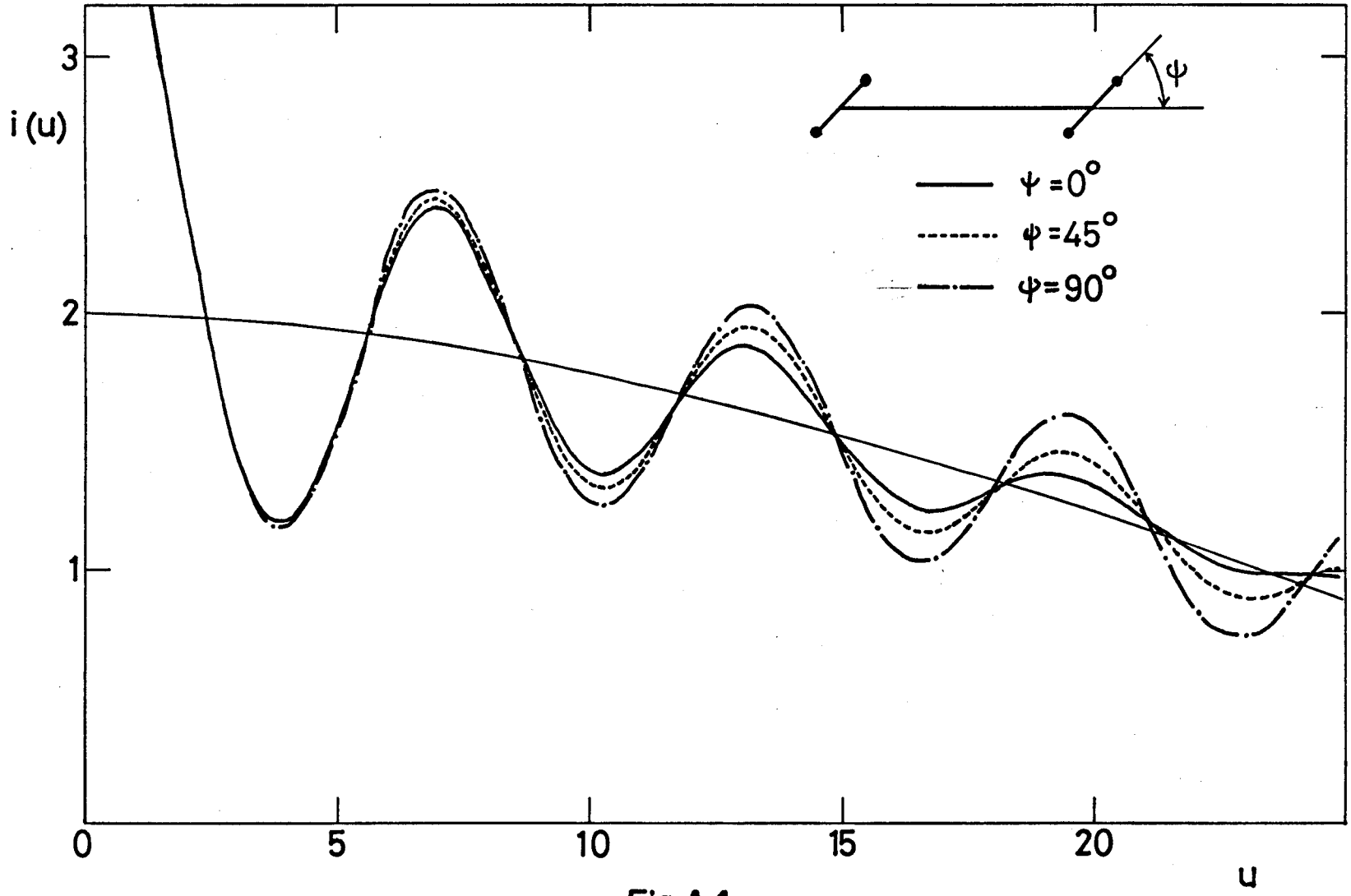

Fig. A4

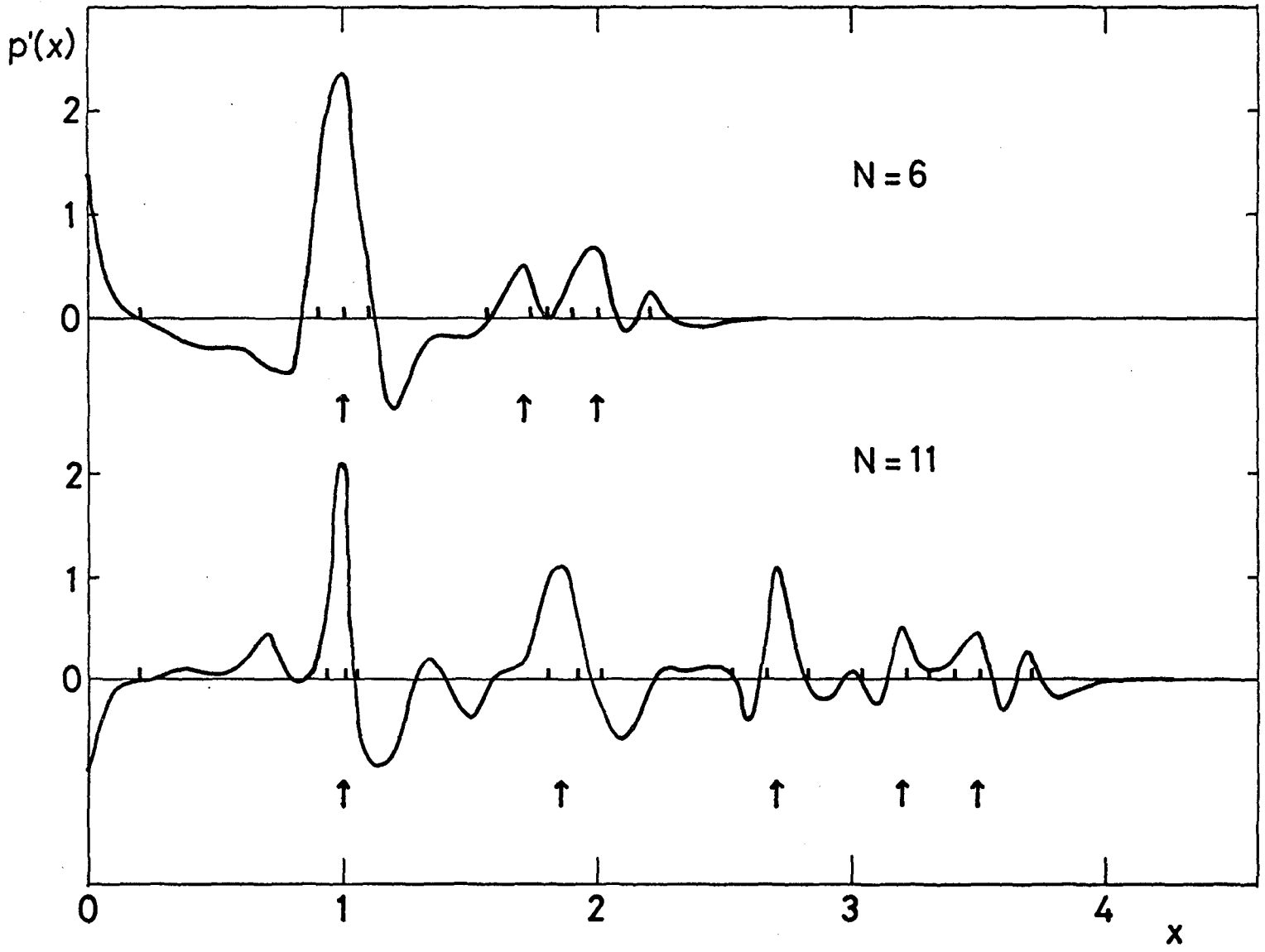

Fig. A5

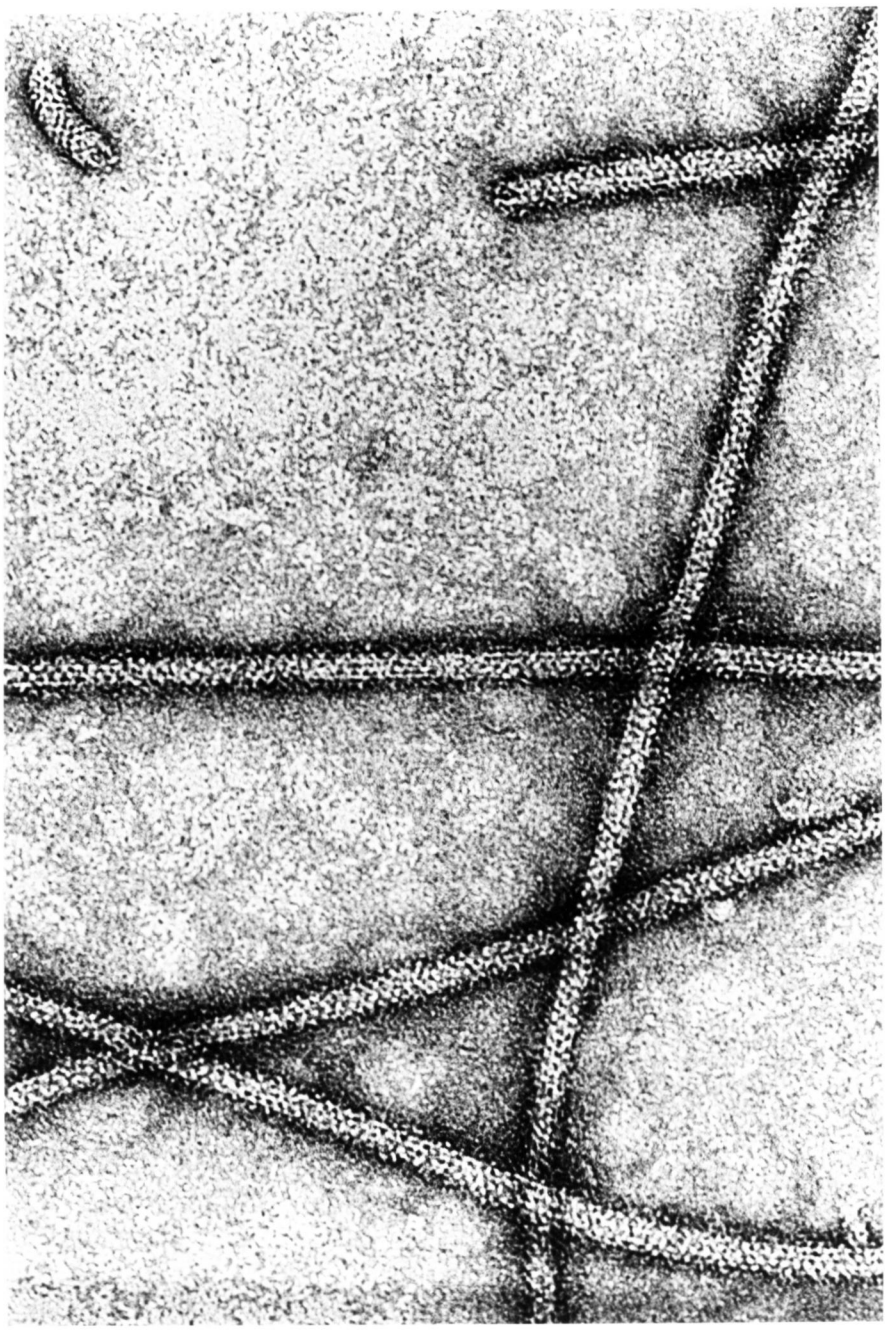

PLATE 1

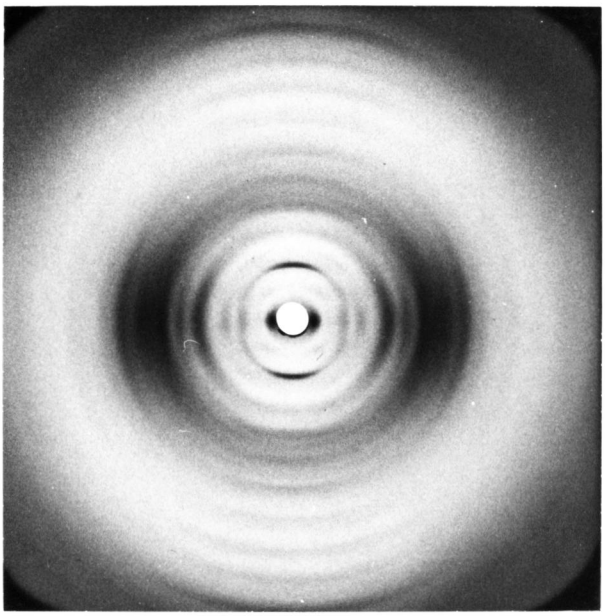

(a)

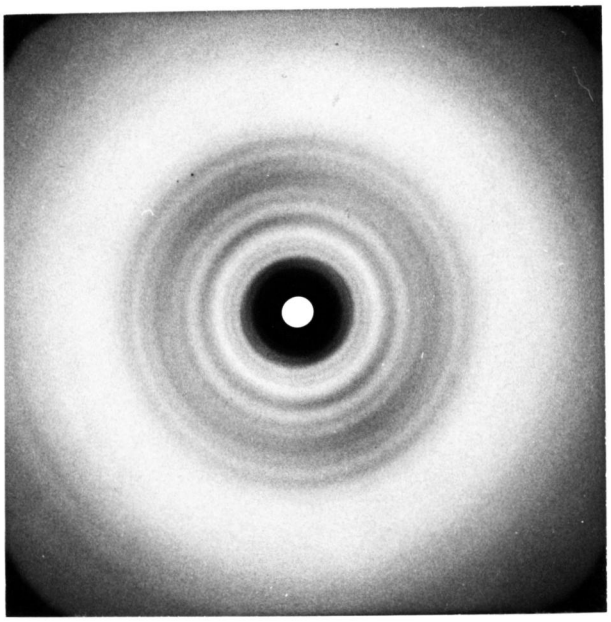

(b)

PLATE 2